Experience-Dependent Plasticity in Nucleus Laminaris of the Barn Owl

Catherine E. Carr[1], Tiffany Wang[1], Ira Kraemer[1], Paula T. Kuokkanen[2], Grace Capshaw[3], Go Ashida[4], Richard Kempter[2], Christine Köppl[4]

[1]Department of Biology, University of Maryland College Park, College Park, MD 20742 USA

[2]Institute for Theoretical Biology, Department of Biology, Humboldt-Universität zu Berlin, Berlin, Germany

[3]Department of Psychological and Brain Sciences, Johns Hopkins University, Baltimore, MD, USA.

[4] Department of Neuroscience, School of Medicine and Health Sciences, , Research Center for Neurosensory Sciences and Cluster of Excellence "Hearing4all" Carl von Ossietzky University, 26129 Oldenburg, Germany.

6 Figures

3 Tables

Key words: Auditory, development, ABR, barn owl

Corresponding author:

Catherine Carr

Department of Biology, University of Maryland College Park, College Park, Maryland USA 20742, USA.

Phone: 1-301-405-6915

Email: cecarr@umd.edu

Abstract

Barn owls experience increasing interaural time differences (ITDs) during development, because their head width more than doubles in the month after hatching. We therefore hypothesized that their ITD detection circuit might be modified by experience. To test this, we raised owls with unilateral ear inserts that delayed and attenuated the acoustic signal, then used the binaural neurophonic to measure ITD representation in the brainstem nucleus laminaris (NL) when they were adult. The ITD circuit is composed of delay line inputs to coincidence detectors, and we predicted that plastic changes would lead to shorter delays in the axons from the manipulated ear, and complementary shifts in ITD representation on the two sides. In owls that received ear inserts around P16, the maps of ITD shifted in the predicted direction, but only on the ipsilateral side, and only in those regions that had *not* experienced auditory stimulation prior to insertion. The contralateral map did not change. Thus, experience-dependent plasticity of the ITD circuit occurs in NL, and our data suggest that ipsilateral and contralateral delays are independently regulated. Thus, altered auditory input prior to, and during, sensory experience leads to long lasting changes in the representation of ITD.

Introduction

Barn owls (genus *Tyto*) are altricial, blind and deaf when they hatch (Haresign and Moiseff, 1988; Köppl et al., 2005). Young barn owls begin to acquire auditory sensitivity around day 4 posthatch (P4), their eyes open by about P10, their heads grow to adult width by about P30, and the growth of their facial ruff and sensitivity to high frequency sounds is complete by about P60 (Haresign and Moiseff, 1988; Rich and Carr, 1999a; Köppl et al., 2005; Campenhausen and Wagner, 2006; Kraemer et al., 2017). Thus, the early life of barn owls is marked by increasing sensitivity to sound, and by increasing interaural time and level differences. This prolonged post-hatch development allowed us to examine the role of altered auditory experience on the ITD detection circuits.

Detection of ITDs depends on precise coding of ongoing phase delay by the inputs to postsynaptic coincidence detectors in the nucleus laminaris (NL) which in turn depends on highly specialized morphology and physiology of its circuit elements (Carr and Konishi, 1990; McColgan et al., 2014; Carr et al., 2015). Previous studies had shown that this ITD detection circuit matures slowly (Kubke and Carr, 2000), and we hypothesized that neural delays might be modified by experience (Cheng and Carr, 2007). The adult NL contains large, well-ordered maps of ITD, which we exploited to test this hypothesis. We reasoned that, if axonal delay lines adjusted to temporally altered acoustic input, then the maps of ITD would be shifted compared to normal. To test this hypothesis, we first described the maps of ITD precisely (McColgan et al., 2014; Carr et al., 2015), then fitted 8 young owls (from P21) with unilateral ear-canal inserts (acoustic filtering devices) designed to introduce a time delay to inputs from that ear (Gold and Knudsen, 1999; Köppl et al., 2012), and later compared their ITD maps with those of normal adult owls. The manipulated owls did not show altered maps of ITD (Köppl et al., 2012). Although abnormal auditory experience starting around P25 induces adjustments in tuning for binaural localization cues in owl midbrain (Gold and Knudsen, 1999, 2000a, 2000b), we reasoned that P21 might be past a critical period for adjustment of delays in the brainstem NL. We therefore raised 6 owls from about P14 with unilateral earmold plugs, and report on the results of both studies here.

Multiple critical periods have been documented at different levels of the auditory system (Polley et al., 2013; Persic et al., 2020). Early in development, before the emergence of hearing, waves of synchronous activity propagate through the developing auditory brainstem and are hypothesized to refine the tonotopic maps that define these circuits (Friauf and Lohmann, 1999; Jones et al., 2001; Kandler et al., 2009; Sonntag et al., 2009; Clause et al., 2014; Babola et al., 2018). Upon hearing onset, connections in brainstem nuclei are rapidly refined, and at this time appear most vulnerable to disruption by deafening and noise rearing (Kapfer et al., 2002; Werthat et al., 2008; Kandler et al., 2009; Sonntag et al., 2009;

Popescu and Polley, 2010; Butler and Lomber, 2013; Polley et al., 2013; Clarkson et al., 2016; Babola et al., 2018; Persic et al., 2020). Many synaptic and ionic mechanisms contribute to observed refinement and can exhibit their own patterns of maturation (for reviews see (Trussell, 1999; Sanes, 2002; Kandler and Gillespie, 2005; Kubke and Carr, 2006; Tzounopoulos and Kraus, 2009; Klug et al., 2012; MacLeod and Carr, 2012; Ngodup et al., 2015; Kohrman et al., 2021)). The onset of phase locking appears to follow closely upon hearing onset (Sanes, 1993; Brenowitz and Trussell, 2001; Crins et al., 2011; Dyke et al., 2017). Phase locking is a prerequisite for ITD detection since precise timing of binaural inputs underlies coincidence detection. We assume here that the onsets of hearing and phase locking are close together in time in the barn owl (Köppl, 2007).

Unilateral hearing loss has profound effects on binaural circuits (Moore et al., 1999; Moore and King, 2004; Sanes and Bao, 2009; Popescu and Polley, 2010; Persic et al., 2020). Recent reviews have outlined the effects of hearing loss on auditory brainstem plasticity (Sanes and Bao, 2009; Tzounopoulos and Kraus, 2009; Anderson et al., 2010; Keating and King, 2013; Friauf et al., 2015; Lauer et al., 2019; Persic et al., 2020; Rubio, 2020), and upon localization behavior in rats ((Clements and Kelly, 1978), ferrets (Moore et al., 1999; Keating and King, 2013; Kumpik and King, 2019), gerbils (Maier et al., 2008) and barn owls (Knudsen, 2002; Bergan and Knudsen, 2007; Keuroghlian and Knudsen, 2007). Previous studies have shown clear refinement of inputs to the ITD sensitive neurons of the mammalian medial superior olive (Kapfer et al., 2002; Chang et al., 2003; Magnusson et al., 2005; Werthat et al., 2008; Winters and Golding, 2018).

In the present study, we examined the effects of unilateral hearing loss on ITD coding *in vivo* in NL, the first binaural nucleus in the barn owl. These recordings were possible because NL is large and has reproducible maps of ITD (Carr et al., 2015). The maps are created by afferent delay lines whose responses sum in NL to create a binaural ITD-sensitive neurophonic (kuokkanen 2013). Recordings from these well-ordered maps allowed for detection of the small ITD shifts associated with conductive hearing loss.

Methods

All experiments were carried out on barn owls of both sexes. Recordings from American barn owls (*Tyto furcata;* previously classified as *Tyto alba pratincola*) in Maryland conformed to procedures in the NIH Guidelines for Animal Research and were approved by the Animal Care and Use Committee of the Universities of Maryland. Experiments in Oldenburg were carried out on European barn owls *(Tyto alba)* following protocols and procedures approved by the authorities of Lower Saxony, Germany (permit No. AZ 33.9-42502-04-11/0337).

Acoustic Filtering Devices

In our first experiments (Köppl et al. 2012), owls (n=8, 2 *T. furcata* and 6 *T. alba*) were raised with acoustic filtering devices (Gold and Knudsen, 1999). Two owls (*T. furcata*) were first binaurally occluded with dense foam rubber earplugs (E.A.R. Cabot) to limit auditory experience from 20 to 28 days of age (P20-P28), corresponding to the time that their ear canals were open but too narrow to accommodate the device. Around 29 days of age, the binaural foam plugs were removed, and the filtering device was sutured into the right ear canal. The other 6 (*T. alba*) were raised beginning with a modified acoustic filtering device that could fit a younger ear canal (5.5 - 7.5 mm diameter of the ear-canal part), which was then replaced with a full size (8.5 mm diameter) device when the ear canals were large enough (Table 1). The foam earplugs and the acoustic filtering devices were sutured into place while the owls were anesthetized with isofluorane (1-2%). The acoustic filtering device was designed by Gold (Gold and Knudsen, 1999) to alter auditory experience, and custom-made from acetal delrin (Plastics SRT). A small, circular flange fit tightly to the inner walls of the ear canal, and the rest of the device was located just behind the preaural flap and in front of the facial ruff feathers. The device was designed to increase the

path length of sound reaching the affected ear and to change the resonance properties of the ear canal while still providing a low- impedance pathway to the tympanic membrane. One owl (*T. alba*) was raised with an early version of the filtering device that had a shorter and smaller diameter chamber; the acoustic properties of this device were not measured. All 8 owl chicks were raised to minimum age of 3 months wearing the devices (see Table 1).

Since the acoustic filtering device did not appear to affect the map of ITD in the NL, a further 6 owl chicks (*T. furcata*) were raised with unilateral impression earmold plugs (Gold Velvet, Oklahoma City) inserted into the left ear canal under 1% isofluorane anesthesia. These earmold plugs could be inserted at an earlier age (around P14) to limit auditory experience. Starting at P14, the average diameter of the ear canal was about 1.8 mm, increasing to about 6.2 mm at day 30 (Haresign and Moiseff, 1988). During this first month after hatching, the ear opening diameter increases fairly linearly ($y = 0.2x - 0.25$), and it was possible to insert an earmold plug after about P14. The 6 owls, plus 2 age matched controls, were hand-raised in a Brinsea TLC-4 incubator (N. Somerset, UK), with temperature adjusted every few days as their thermoregulation ability increased (Rich and Carr, 1999b). The earmold plugs were examined daily and replaced every few days as the ear canals grew until the owls were about 3 months old. The plugs were then removed and the owls were returned to the aviary to reach adulthood (> 6 months), after which their maps of ITD were measured. Block of the middle ear was not possible because the large interaural canal that connects the two ears (Gans et al., 2012; Kettler et al., 2016).

Manipulation	**Age at which plug/device first applied**	**Duration**	**N**
Foam plug followed by device	P20-28 (soft plug) P29 (device)	3-6 months	2 *T. furcat*a
Small (5.5 - 7.5 mm diameter) device followed by 8.5 mm device	P20-27 (small device) P26-33 (device)	3-6 months	6 *T. alba*
Ear mold plug	P14-17 (replaced with growth)	3 months	6 (*T. furcata*)

Table 1. Ear plug manipulations

Auditory Brainstem Responses (ABR)

To determine if plug rearing led to long lasting changes in sensitivity,we used auditory brainstem responses (ABRs) to measure sensitivity in free field in 4 adult owls that had been raised with an earmold insert, and in 4 age matched controls (Fig. 1A). The plugs were removed prior to ABR recordings. For comparison with previous measurements, we used the same protocol and equipment as in (Kraemer et al., 2017). Owls were anesthetized by intramuscular injection of xylazine and ketamine. Doses were calculated using the weight formula (0.0004*weight (kg) = X mL 20mg/ml xylazine, 0.00025*weight (kg) = X mL 100mg/ml ketamine). Owls were placed in a large anechoic chamber (I.A.C.), wrapped in a heating blanket (38°C) with their head positioned 30 cm away from the speaker. Lidocaine was applied to the skin prior to inserting the electrodes subcutaneously. TDT software BioSigRP was used to present stimuli and record from the three platinum subdermal needle electrodes. The negative electrode behind the ear facing directly towards the speaker, the ground electrode behind the opposite ear, and the active electrode directly on the midline vertex of the barn owl's head. We used SigGenRP software (Tucker-Davis Technologies, Gainesville, Florida) to create tone-burst stimuli, which were fed through an RP2.1 (TDT). The electrode signal was processed using a Medusa Digital Biological Amplifier System (RA4L Head stage and RA16PA PreAmp, RA16BA Medusa Base station). After data collection, the signals were notch filtered at 60 Hz, low-pass filtered at 3000 Hz, and high-pass filtered at 30 Hz in the "BIOSIG" software. Thresholds for clicks and individual frequencies were established as the lowest stimulus level where any recognizable feature of the waveform was discernible, using visual inspection (Kraemer et al., 2017). Thresholds were defined as the decibel level between the trace with a detectable peak and the trace

without a detectable peak, so were either 5 dB or 2.5 dB SPL below the detectable peak. At least two thresholds (from 300 stimulus repetitions each) were determined for each frequency per trial. Thresholds were then averaged for each bird. ABR audiograms from owls raised with an earplug were not statistically different from the normal population except for the 0.5 kHz point in the plug reared owls and the 6.3 kHz point in the control group. A one-way ANOVA revealed a statistically significant difference in threshold between the two groups ($F(7) = 12.715$, $p = 0.012$).

We also measured the effect of acute earmold plug insertion (unilateral and bilateral) in 2 P21 owls to determine the degree of attenuation caused by the earmold plugs around the time of insertion (Fig. 1B, C). We used the same ABR setup as before, with free field stimulation. We therefore measured the effect of both monaural and binaural earplug insertion and compared normal ABRs with ABRs recorded with bilateral and unilateral plugs (Fig. 1B). Above 2 kHz, mean bilateral attenuation for P21 animals was 16±3 dB, and for adult owls 17±4 dB (data not shown). An unbalanced one-way ANOVA showed significant differences in detection thresholds between normal and earplugged conditions for frequencies between 0.5-8 kHz in the adult owl ($F_{1,13}$ =19.47, $p<0.0007$, not shown), and for frequencies between 0.5-6.3 kHz in the P21 chick ($F_{1,10}$ =9.16, $p<0.013$, data in Fig. 1B, compare P21 bilateral and no plug).

Surgery and stereotaxis

To measure neurophonic potentials in NL, most animals were examined over 2 or 3 separate 8-hour experiments, spaced approximately a week apart, and designed to follow the protocols used in (Köppl et al., 2012; Carr et al., 2013, 2015). Anesthesia was induced by intramuscular injections of 16 mg/kg/hr ketamine hydrochloride ("Ketavet" Phoenix, St. Joseph, MO) plus 3 mg/kg/hr xylazine ("Xyla-ject", Phoenix). Supplementary doses of ketamine and xylazine were administered to maintain a suitable plane of anesthesia. Body temperature was measured by a cloacal probe and kept constant at 39ºC by a feedback-controlled heating blanket wrapped around the owl's body (Harvard Instruments, Braintree, MA). An electrocardiogram was used to monitor the plane of anesthesia.

Initially, the owl's head was firmly held in a controlled position by a custom-designed stereotaxic apparatus, using ear bars and a beak holder designed to position the head at 70° to the visual axis. Then a metal head plate and marker of a standardized zero point was permanently glued to the skull. After this, the ear bars and beak holder were removed, and the head held by the head plate alone. A craniotomy was made around the desired area relative to the zero point and a small hole made in the dura mater, taking care to avoid blood vessels. Each electrode was positioned at defined rostrocaudal and mediolateral locations, before being advanced into the brain. In some cases, the electrode was angled to facilitate access to the most medial regions of the brainstem.

Electrodes and recording

Owls were placed on a vibration-insulated table within a sound-attenuating chamber (IAC, New York) that was closed during all recordings. Generally, commercial, Epoxylite coated tungsten electrodes (Frederick Haer Corporation, ME) were used, with impedances between 2 and 20 MΩ and generally 250 µm diameter shank (see Figure 8G in (Kuokkanen et al., 2010). A grounded silver chloride pellet, placed under the animal's skin around the incision, served as the reference electrode. Extracellular electrode signals were amplified and filtered by a custom-built headstage and amplifier (mA 2000, Walsh Electronics, Pasadena, CA). Recordings were passed in parallel to an oscilloscope, a threshold discriminator (SD1, TDT, Tucker-Davis Technologies, Sarasota FL) and an analogue-to-digital converter (DD1, TDT) connected to a personal computer via an optical interface (OI, TDT). Analogue waveforms were saved for offline analysis.

Stimulus generation and calibration

For neurophysiological recordings, acoustic stimuli were digitally generated by custom-written software ("Xdphys" written in Dr. M. Konishi's lab at Caltech, CA) driving a signal-processing board (DSP2, TDT). After passing a digital-to-analogue converter (DD1, TDT) and an anti-aliasing filter (FT6-2, corner frequency 20 kHz, TDT), the signals were variably attenuated (PA4, TDT), impedance-matched (HB6, TDT) and attenuated by an additional fixed amount before being fed to commercial miniature earphones. Two separate channels of signals could be generated, passing through separate channels of associated hardware and driving two separate earphones (Yuin PK2, China). The earphones were housed in custom-built, calibrated from 0.1-10 kHz, closed sound systems inserted into the owl's left and right ear canals, respectively. Sound pressure levels were calibrated individually at the start of each experiment, using built-in miniature microphones (Knowles EM3068, Ithasca, IL). The analogue stimulus waveforms were saved in most experiments.

Acoustic stimuli

Acoustic clicks, noises, and tone stimuli were digitally created with a sampling rate of approximately 48 kHz (exact sampling interval: 20.8 µs). Clicks were digitally produced and then processed by the TDT-systems (Wagner et al., 2005, 2009). Several parameters of the click stimulus could be varied: intensity (maximally 0 dB attenuation, corresponding to 65 dB SPL spectrum level at 5 kHz (34 dB SPL overall level)), duration (1-4 samples equivalent to 20.8 - 83.2 µs), and polarity. A condensation click at 0 dB attenuation and 2 samples duration served as a reference. The click stimulus was repeated 128 times. Tone bursts of different frequencies (500 – 10,000 Hz range, 50 - 500 Hz steps) were presented monaurally and binaurally at levels from 20 - 60 dB SPL. Tone burst duration was 100 ms with 5 ms rise/fall times and a constant starting phase.

Recording protocol

While lowering the electrode, noise bursts were presented as search stimuli. Once auditory neurophonic responses were discernable, tonal stimuli of varying frequencies were applied from both the ipsi- and contralateral side to judge the position of the electrode. To map best ITD within an isofrequency band, we made multiple stereotaxically controlled penetrations through the overlying cerebellum into NL. Apart from low-frequency NL, which has a lateral bend where frequencies from 500 - 2,000 Hz are represented (Takahashi and Konishi, 1988; Köppl, 1997, 2001), NL is sufficiently large and ordered for 3 - 4 serial penetrations along the same isofrequency slab within an 8-hour experimental period.

At a given recording site, the following protocol was tested to obtain a data set. To determine best frequency, average threshold crossings of the neurophonic potential in response to 3 - 5 repetitions of each stimulus were calculated within the stimulus window. This paradigm was chosen to derive iso-intensity frequency response curves for best frequencies between 2 - 7.5 kHz. Best interaural time differences (ITDs) were determined using two assumptions; first, that ITD tuning changed continuously with depth. Second, that ITDs at or close to 0 µs would occur within a penetration (a best ITD of 0 µs). Best ITD were calculated from responses to either tone bursts presented binaurally at the estimated best frequency or to stimulation with noise bursts. The noise had a spectrum between 0.1 and 13 kHz, 5-ms rise/fall times, and duration of 100 ms. The overall level of the noise varied between 20 - 60 dB SPL. ITDs generally covered about two periods at the best frequency of a location. The tuning to ITD was judged by a Rayleigh test ($p < 0.05$). We recorded from both sides of the brain, with left ear leading ITDs described as negative, and right positive.

Data analysis

A brief signal analysis was done during the experiment to determine frequency and ITD tuning. After the experiment, the responses were quantitatively analyzed with custom-written software (MATLAB; BEDS

scripts from G. B. Christianson). Frequency and ITD tuning were quantified using the variance of the ongoing neurophonic response; onset effects were excluded, and we averaged the variance over several trials. Only those recordings with both frequency and ITD tuning (Kuokkanen et al., 2013; Carr et al., 2015) were accepted. The vector strength (vs) of the ITD tuning of the response variance was evaluated at each recording depth, and required to be > 0.02 and significant at $p < 0.05$ (Kuokkanen et al 2010).

BF tuning curves at sites with weak neurophonic ITD tuning were included if there was a strong ITD tuning of the cyclic mean amplitude (Kuokkanen et al 2010, 2013) of vs > 0.1 and $P<0.005$. The monaural frequency-response curves were typically recorded multiple times during a penetration, and the maximum Signal to Noise Ratio (SNR_{max}) was required to be at least 10 dB within the range of stimulus frequencies for both stimulus sides. We also cross-correlated the frequency response curves to ipsilateral and contralateral stimulation at each recording site to determine if there were a relationship between interaural mismatches in frequency tuning and ITD tuning. The BF response curves were linearly interpolated between stimulus frequencies to about 1-5 Hz resolution to ensure a smooth cross-correlation curve. The frequency-lag at the maximum of the cross-correlation was used to describe the shift between the tuning curves.

Statistics

We evaluated the effects of monaural occlusion on best frequency and best ITD using linear mixed-effects modeling in R statistical software (lme4 package). Linear mixed-effects models were chosen because they are robust to missing data and unbalanced designs. The SNR_{max} of the neurophonic potential was incorporated as the response variable in each model, and recording side, best frequency (BF-) population (high or low BF frequency regions of NL) , and their interaction (side x BF-population) were included as fixed effects. All earmold plugs were placed the left ear, to simplify analysis. Thus L_{brain} $L_{stimulus}$ means recording from the side with plug, with ipsilateral stimulation, while L_{brain} $R_{stimulus}$ means recording from the side with plug, with contralateral stimulation. The data were divided into low (≤5 kHz) and high (> 5 kHz) BF groups based on the stimulus frequency of the maximum SNR and stimulus frequency of the ITD tuning curve. We incorporated subject ID as a random effect in each model to account for individual variation. Post-hoc analyses of significant fixed effects were performed by computing the estimated marginal means (i.e., least-square means) of linear mixed-effects models and examining pairwise comparisons among groups using the R package emmeans.

Electrolytic lesions and histology:

Lesions (10 µA, 3-10 s) were made at locations closest to 0 µs best ITD using a constant current device (CS3, Transkinetics, Canton, MA, or Lesion Making Device, Ugo Basile, Gemonio, Italy). After a survival time of 5 - 14 days, owls were perfused transcardially with saline, followed by 4% paraformaldehyde in phosphate buffer. Brains were blocked in the same stereotaxic apparatus as for *in vivo* recordings, marked on either left or right side, then cut in the transverse plane orthogonal to the electrode penetrations. Forty micron sections were mounted on gelatin-coated slides and stained with cresyl violet. A trained observer, blinded to condition, examined all sections at low magnification to identify electrode tracks and lesions, and then visualized and reconstructed every 3rd section using a Neurolucida neuron tracing system (Microbrightfield Bioscience, St Albans, VT) that included an Olympus BX61 light microscope, a video camera (MBF-CX9000, Microbrightfield), a motorized stage controller, and a personal computer. Sections were traced and digitized directly on the microscope using a 10x objective, with the Z-position defined based on the thickness of each slice. Each section was aligned with the previous slice using rotation, reflection, or translation only. Lesions, lesion tracks, and NL borders were marked using the tracing function. The ruler function was used to measure distances from the lesion center to the borders of the nucleus. The distance of each lesion along its isofrequency band was measured from 3D reconstructions of NL. Isofrequency bands traverse NL and are composed of inputs from the nucleus magnocellularis with similar best frequency (Carr et al., 2015). Sections were not

corrected for shrinkage (Kuokkanen et al., 2013) since measurements were normalized. Lesions varied in size, from 60 - 270 µm diameter (mean ± SD = 190 ± 64 µm, n = 61, Figures 3 and 4).

Results

Since the development of stable ITD cues coincides with development of brainstem auditory circuits, we hypothesized that delays might be modified by experience (Fig. 2). We used the accessible map of ITDs in the NL to test this hypothesis in young owls raised with unilateral earplugs. (Gold and Knudsen, 1999; Popescu and Polley, 2010) Both types of inserts attenuate as well as delay the acoustic stimulus to the manipulated ear, in a frequency specific manner. It is important to note that ITD coding by the brainstem NL is based on phase-locked neural inputs whose preferred phase is basically invariant with sound level (review: Heil and Peterson, 2015; barn owl: Köppl, 1997b; Wagner et al., 2005). Thus, although acoustic attenuation will additionally delay neural onset responses (Wagner et al., 2005), this effect is predicted to be negligible here, and the dominant effect of the ear inserts is assumed to be a unilateral, frequency dependent phase shift of the neural inputs to the developing NL on both sides of the brainstem. We predicted that, if compensation were to occur, the manipulated-ear inputs should become "faster", i.e. show a decrease in delay when the plug is removed. If compensation were comprehensive, changes of up to 50 µs are to be expected which corresponds to the typical acoustic delay effected by the ear inserts for frequencies up to 5-6 kHz (Knudsen et al., 1984; Gold and Knudsen, 1999). At still higher frequencies, the introduced acoustic delays are smaller. We tested this hypothesis by looking for a shift in the map of ITD after the auditory system matured. From dorsal to ventral in brainstem recordings, the NL contains an ordered representation of contralateral ITDs and a smaller representation of ipsilateral space, covering a total range of ~200 µs ITD (Carr et al., 2015). Thus, a "faster" ipsilateral input should cause the representation of frontal space, around 0 µs ITD, to be represented significantly more ventrally within NL, when tested with the ear insert removed (Fig. 2D). We had previously characterized the normal ITD map to be able to determine if changes in early experience led to long lasting changes in the brainstem map of ITDs (McColgan et al., 2014; Carr et al., 2015).

Owls Raised with an Early inserted Unilateral Earmold Plug had Altered Maps of ITD

To measure the effect of plug raising on the development of the map of ITD, we compared ITD maps in normal owls (Carr et al., 2015) with maps recorded in 6 owls raised with an earmold plug. In normal owls, ITD maps show a steady shift in the position of 0 µs best ITD in the mediolateral dimension within any isofrequency slab (Fig. 2). Thus, 0 µs best ITD is mapped dorsal in medial NL and ventral in lateral NL (Carr et al., 2015). In normal owls, this shift is described by a regression of $y = -0.74x + 0.78$, $R^2=0.64$ (Figures 2B red line, 6B black line, Carr et al., 2015).

It is possible to detect microsecond shifts in best ITD in the experiments in barn owls raised with an earplug because the ITD maps recorded in NL are highly reproducible (Sullivan and Konishi, 1986; Wagner et al., 2005; Carr et al., 2015) (Fig. 2A). We identified the 0 µs points as precisely as possible using online analyses (mean = -3.8 ±5.5 µs, n=61) prior to making a lesion. The best ITDs were confirmed off-line using measures of signal to noise (SNR (Kuokkanen et al., 2010)) and found to be close to the online measurements (mean = -5.7±10.0µs, mean difference 1.8±7.3 µs, n=61). We reconstructed the lesion locations to determine if there were changes in the map of ITDs (Fig. 3A, B).

If the maps of ITD were to adapt to decreased sensory experience from the plugged ear, we predicted that a decrease in delay could create a normal map (Fig. 2) that would be revealed by a ventral-ward shift in the map of ITD on the side with the hearing loss, after the plugs were removed (Fig. 2D). On the brainstem side contralateral to the earmold plug, a decreased contralateral delay (mediated by the same NM neurons on the manipulated side) would then cause an equal and opposite dorsal-ward shift in the maps of ITD. In other words, we hypothesized that the maps of ITD in the ipsilateral and contralateral NL would shift in opposite directions. We quantified the maps of ITD as above and found evidence for

plastic shifts in the maps of ITD in the owls raised with an earmold plug. In these owls, the maps of best ITD ipsilateral to the earmold plug were shifted ventrally, consistent with the prediction (Fig. 2D), but the maps of ITD contralateral to the earmold plug were unaffected, not consistent with the prediction of change on both sides.

NL is tonotopically organized, with low best frequencies mapped caudally, and progressively higher frequencies rostrally. A band across the mediolateral dimension of NL, oriented along a diagonal of about 45° to the midline, represents a single frequency and is referred to as an isofrequency band (Takahashi and Konishi, 1988; Carr and Konishi, 1990; Carr et al., 2013). We made multiple penetrations through the short, dorsoventral axis of NL within each isofrequency band to measure ITD tuning (Fig. 2, 3A), both ipsilateral and contralateral to the side that had experienced the earmold plug. We could not be blind to the side of the earplug, but analyses of lesion positions were blinded (Fig. 3). In birds raised with an earmold plug we found a systematic ventral-ward shift in the representation of 0 µs best ITD in the NL, ipsilateral to the earmold plug (Fig. 3C). The maps of ITD in the contralateral NL were not statistically different from the normal maps of ITD (Fig. 3D), i.e. they shared similar slopes and y-intercepts to those of the control owls (Carr et al., 2015). Furthermore, whether the maps shifted depended on the tonotopic region examined (Fig. 3C). Only ITD maps in the high best frequency region of NL showed plastic shifts.

Maps of ITD were not plastic after the onset of hearing

At first, we combined results from all iso-frequency bands because, in normal birds, the range of ITDs did not change with frequency, at least within the 3-8 kHz range examined (Carr et al., 2015). However, we were only able to insert the earmold plug around P14-18, or around the age when the owl chicks could hear frequencies between 500 Hz-5 kHz (Köppl and Nickel, 2007; Kraemer et al., 2017). We therefore re-analyzed the data and separated the results by frequency, i.e., position along the tonotopic axis. The ITD maps from the 3-5 kHz regions of NL were not different to the normal ITD map while the ITD maps from 5-7.5 kHz were shifted ventral (Fig. 2D, 3C). The slopes of each regression were not different, but the y-intercepts were, suggesting a ventral-ward shift of about 30%, corresponding to a shift in best ITD of approximately 50 µs. Since owls only begin to hear frequencies above 5 kHz after P16 (Köppl and Nickel, 2007; Kraemer et al., 2017)), these results were consistent with the prediction that only a brief period of auditory experience was required for the neural delay lines in the ITD circuit to finally mature.

Balance of ipsi- and contralateral inputs

We next compared the strength of the inputs to the coincidence detectors from each side. We compared both the BF- and the ITD-sensitivity of the neurophonic responses in low-BF (unshifted) and high-BF (shifted) regions of NL with matching responses from the contralateral NL, and with measurements from age-matched controls (Fig. 4). Computational modeling and analysis of monaural neurophonic responses have shown that the neurophonic potential in NL is generated by hundreds of statistically independent sources, suggesting the afferent delay lines from the nucleus magnocellularis are its primary contributors (Kuokkanen et al., 2010, 2013, 2018). We therefore used the neurophonic to quantify the strength of the response from each ear, using the signal to noise (SNR) of the monaural neurophonic responses to tones. This allowed us to compare ipsi- and contralateral inputs to NL on both sides of the brainstem (plug and no plug sides), and to compare these with age-matched controls (Fig. 4). These analyses helped to separate the role of location (left NL, ipsilateral to the plug vs. the normal or right NL) from experience (recording from ipsi- and contralateral inputs within each NL, where one input originated from the plug side, and the other from the unmanipulated side).

We assessed the influence of rearing with a unilateral earmold plug on the SNR_{max} of neurophonic responses to monaural stimulation at BF using a linear mixed-effects model incorporating recording side (plug or no plug, each divided into recordings from ipsi- and contralateral inputs on both sides of the

brainstem as described in the methods section), BF-population (above or below 5 kHz), and the interaction of side and BF-population as fixed factors, and subject ID as a random effect. The linear mixed model showed a strong (p<0.0001, Table 2) effect of the earmold plug on SNR_{max}. Post-hoc pairwise comparisons between groups with a Tukey adjustment of p-values for multiple comparisons showed that ipsilateral inputs to NL on the same side as the earmold plug („LL“ in Fig. 4) were significantly weaker than the ipsilateral inputs to the contralateral NL (RR) and also weaker than the age-matched controls (Fig. 4A, E). This effect was strongest for the high-BF population (<0.0001), but also significant for the low-BF population (Table 3). Furthermore, responses originating from the same NM neurons showed reduced SNRs of their axonal arbors on the plug side (LL), but not on the unmanipulated side (RL; P>0.0178), implicating a side-specific or local effect. In summary, the strength of inputs to coincidence detectors in NL on plug side was reduced, with the strongest effect in the high best frequency regions of NL on the plug side (Fig. 4F).

	Sum Sq	**Mean Sq**	**NumDF**	**DenDF**	**F value**	***P***
Recording side	191.314	47.829	4	117	10.516	<0.0001**
BF-Population	2.711	2.711	1	117	0.596	0.4417
Recording side: BF-Population	35.706	8.926	4	117	1.963	0.1047

Table 2. Main effects of Side (plug or no plug) and BF Population (above or below 5 kHz) on SNR_{max}

We also quantified the binaural ITD tuning from both plug and no-plug sides, using SNR_{max} to determine if there were a loss of synchrony associated with plug-rearing. The best ITD of each recording location was determined from the variance of the cyclic-mean signal (Kuokkanen et al., 2018), which corresponded to the circular-mean direction (mean phase) of the variance as a function of ITD (Fig. 5B, D). As before, we used a linear mixed model incorporating recording side (plug or no plug), BF-population (above or below 5 kHz), and the interaction of side and BF-population as fixed effects, and subject ID as a random effect. A statistical test of the model showed significant effects of side (p=0.0176); however, post-hoc pairwise comparisons found significant differences in SNR_{max} among recordings from the plugged and unplugged sides only for the high BF-population (p=0.0273, Fig. 5G). Thus, rearing with a unilateral earmold plug could be associated with a decrease in SNR, again implicating a side-specific local effect.

	Sum Sq	**Mean Sq**	**NumDF**	**DenDF**	**F value**	***p***
Plug_BrainSide	16.576	8.29	2	313	4.093	0.0176**
Population	6.99	6.99	1	313	3.452	0.0641
Plug_BrainSide: Population	3.89	1.95	2	313	0.961	0.3835

Table 3. Main effects of Side (plug or no plug) and BF Population (above or below 5 kHz) on ITD

Finally, the stereausis hypothesis predicts that ITD tuning may be altered if ipsilateral and contralateral inputs originate from different cochlear positions, with different frequency tuning (Shamma et al., 1989; Pena et al., 2001; Carr et al., 2009; Plauška et al., 2017). We therefore investigated the relationship between interaural mismatches in frequency tuning and plug side (Fig. 5H). Ipsi- and contralateral inputs to NL were not always matched in BF, and sometimes the frequency mismatch could be large enough to affect ITD tuning. However, we found no significant differences between ipsi- and contralateral BF in any groups (Fig. 5H, H*), independent of whether there was a plug in one of the ears or not (age-matched control owls). Our data thus suggest that frequency tuning mismatches cannot account for the shifts in ITD tuning associated with rearing with a monaural earmold plug.

Maps of ITD were Unaffected by Rearing with a Unilateral Acoustic Filtering device

Both unilateral acoustic filtering devices and earmold earplugs were used to assess the role of experience in the development of sensitivity to ITDs in NL. The acoustic filtering device increased the path length of sound reaching the affected ear and changed the resonance properties of the ear canal while still providing a low-impedance pathway to the tympanic membrane (Gold and Knudsen (Gold and Knudsen, 1999). These early experiments, however, only yielded an increase in the variability of the map of ITDs (Fig. 6)(Köppl et al., 2012), leading to the hypothesis that brainstem and midbrain auditory circuits experienced different developmental windows for auditory plasticity.

When we used the unilateral acoustic filtering devices to assess the role of experience in the development of sensitivity to ITDs in 8 barn owl chicks, we found similar maps of ITD to the normal maps (Fig. 6B). The normal ITD map is characterized by a steady shift in the position of 0 µs best ITD(Carr et al., 2015), described by a regression of $y = -0.74x + 0.78$, $R^2=0.64$ (Figure 6B, black line). In the owls raised with acoustic filtering devices, the maps of ITD were not statistically different to the normal owls (Fig. 6B, blue lines). The ITD maps did, however, appear to be less organized, i.e., the regressions explained less of the variance.

Discussion

Sensitivity to binaural delays can be modified by conductive hearing loss when an ear is plugged prior to auditory experience (Knudsen et al., 1984; Popescu and Polley, 2010; Kumpik and King, 2019). It was possible to examine the effects of these manipulations at the level of the brainstem in barn owls because of the large size and reproducible nature of the ITD maps in NL (Carr et al., 2015). The maps are created by afferent axonal delay lines whose responses sum in NL to create a binaural ITD-sensitive neurophonic (Sullivan and Konishi, 1986; Wagner et al., 2005, 2009). We found long lasting changes in the map of ITDs associated with a brief window for plasticity around the onset of hearing. Furthermore, shifts in the map of ITDs were restricted to the side of the hearing loss, suggesting independent regulation of ipsilateral and contralateral circuits for detection of ITD.

Effects of Monaural Occlusion

Young owls learn to associate particular ITDs with corresponding locations in space (Keller and Takahashi, 1996; Poganiatz and Wagner, 2001). Knudsen and his colleagues analyzed developmental changes in barn owls under various conditions of monaural occlusion and showed that if an ear is occluded during the first two months of life, owls were able to recover normal localization accuracy while plugged (Mogdans and Knudsen, 1993; Brainard and Knudsen, 1995; Knudsen and Brainard, 1995; Miller and Knudsen, 2003; Bergan and Knudsen, 2007). When the plug was removed, owls showed large errors, but gradually recovered accurate localization (Knudsen et al., 1984). These behavioral changes are associated with significant remodeling of inferior colliculus circuits (for review, see (Knudsen, 2002)).

Knudsen's experiments showed different sites and time constants for plasticity in the circuits for detecting ITDs and interaural level differences (Mogdans and Knudsen, 1993; Gold and Knudsen, 2000b). The first site of binaural interactions in the level difference pathway is the ventral nucleus of the lateral lemniscus (Manley et al., 1988; Mogdans and Knudsen, 1994). A monaural earplug inserted around a month after hatching led to plastic changes in this nucleus that mediated some of the adaptive changes in tuning observed at higher levels of the auditory pathway (Mogdans and Knudsen, 1992). In 1999, Gold developed a phase-shifting acoustic filtering device to examine the plasticity in the barn owl ITD pathway. Rearing with this device inserted monaurally caused remodeling of the projection from the central to external nucleus of the inferior colliculus (Gold and Knudsen, 2000a, 2000b). Gold analyzed the representation of ITD in normal and device-reared owls in the external nucleus, and the lateral shell of the central nucleus, its primary source of input. The external nucleus showed adaptive, frequency-

dependent changes in ITD tuning, while lateral shell responses were unaffected by device rearing. When we raised young owls, using the Gold and Knudsen paradigm, and with device insertion from around P25, we also found no effect of altered auditory experience in the brainstem NL (Köppl et al., 2012), consistent with Gold's findings. These results left unanswered the question of whether the brainstem representation of ITD could be modified by experience. Although the ear canals of younger owls were too small to fit the acoustic filtering device, we were able to induce a monaural conductive hearing loss beginning around P14-16 to reveal plasticity in the brainstem map of ITD. The extent of the shift, about 50 µs, was consistent with the assumed delay imposed by the earmold plugs on the acoustic stimulus (Knudsen et al., 1984). Thus, our data suggest that there are different critical periods for binaural integration in brainstem and midbrain.

Multiple critical periods for binaural integration have been reported in other animal models (for reviews, see (Kumpik and King, 2019). In gerbil auditory cortex, monaural deprivation weakened the effect of inputs from the deprived ear and disrupted binaural integration. Effects were larger in auditory cortex than in the inferior colliculus (Popescu and Polley, 2010; Rosen et al., 2012; Polley et al., 2013; Mowery et al., 2015). In cortex, varying the age of hearing loss onset revealed brief critical periods for membrane and firing properties, as well as inhibitory synaptic currents. These critical periods closed 1 week after ear canal opening (Mowery et al., 2015). In the pallid bat, recordings from auditory cortex revealed different maturation rates for the inhibitory inputs that shape binaural responses (Razak and Fuzessery, 2007). In ferrets, unilateral conductive hearing loss produced long-lasting deficits in binaural hearing (Moore et al., 1999; Kumpik and King, 2019).

We differentiate between the effects of deafferentation and the monaural occlusion model of conductive hearing loss studied here. Rapid and dramatic neuron death occurs after removal of afferent input to the cochlear nucleus and has been carefully examined in both young mammals and birds (for review, see (Parks et al., 2004). Monaural occlusion has been studied in chicks (Tucci and Rubel, 1985), barn owls (Keuroghlian and Knudsen, 2007)and in mammals, principally in ferrets and gerbils (Moore and King, 2004; Moore, 2009; Popescu and Polley, 2010; Kral et al., 2013; Caras and Sanes, 2015; Sinclair et al., 2017; Rubio, 2020). In ferrets, like barn owls, monaural occlusion during infancy led to compensatory changes in auditory spatial tuning that tended to preserve the alignment between the neural representations of visual and auditory space. The key finding was that experience-induced plasticity allows the sound localization circuits to be customized to individual characteristics, such as the size and shape of the head and ears, and to compensate for natural conductive hearing losses, including those associated with middle ear disease in infancy (King et al., 2000).

In gerbils, monaural occlusion has well-defined effects upon the brainstem circuits for detection of ITD. Experiments with earplugs, monaural deafening and noise rearing in gerbils all support a role for experience dependent segregation of inhibition to medial superior olive cell bodies (Kapfer et al., 2002; Maier et al., 2008; Werthat et al., 2008; Sinclair et al., 2017). Recordings from the medial superior olive's target, the nucleus of the lateral lemniscus, related ITD sensitivity to the maturation of inhibitory inputs to the medial superior olive (Seidl and Grothe, 2005). Thus, both *in vivo* recordings from the dorsal nucleus of the lateral lemniscus and studies of the medial superior olive support a role for experience-dependent refinement in the medial superior olive in the first days after hearing onset.

Development of Auditory Sensitivity

To understand the effects of conductive hearing loss, or other modifications of the external ear during development, it is important to know when animals can hear what. In both birds and mammals, auditory responses typically begin with a restricted range of low to mid-frequencies (Romand, 1979; Brugge, 1983; Arjmand et al., 1988; Rubel et al., 1988; Sarro and Sanes, 2010). In the progression to adult hearing, threshold development can be frequency dependent. In cats, high frequency thresholds reach adult levels before low frequencies (Walsh et al., 1986a), while gerbils show faster maturation at the

middle frequencies, with low and high frequencies developing at similar but slower rates (McFadden et al., 1996). Rates of threshold maturation also differ, depending upon where the animal falls along the altricial to precocial spectrum. Some mammals, such as guinea pigs (Dum, 1984) and humans (review in (Werner, 2007), are born with functioning auditory systems and are considered precocial with respect to hearing. Other mammals, such as gerbils (McFadden et al., 1996), ferrets (Moore, 1982) and cats (Walsh et al., 1986a, 1986b), are considered deaf at birth and altricial with respect to hearing. This deafness is relative; closed ear canals in altricial animals muffle sounds, but loud sounds can activate the auditory system (Pujol and Hilding, 1973; Beatty, 1998; Wess et al., 2017).

Birds show a low to high frequency pattern of auditory maturation (review in (Kubke and Carr, 2000, 2006). Precocial birds respond to sound in the egg (Konishi, 1973; Gray and Rubel, 1985; Jones and Jones, 1995; Sato and Momose-Sato, 2003; Mann and Kelley, 2011; Rivera et al., 2018) with adult-like thresholds to low and middle frequencies by the time of hatching, and sensitivity to higher frequencies continuing to improve after hatching (Saunders et al., 1973). Altricial birds, such as the barn owl (Köppl and Nickel, 2007), budgerigar (Brittan-Powell and Dooling, 2004), and pied fly catcher (Aleksandrov and Dmitrieva, 1992) show similar patterns, except that the maturation occurs after hatching (for review, see (Bolhuis, 1991).

When barn owl chicks hatch, they are insensitive to sound, and first show auditory responses to 1-2 kHz around P4-P7 (Köppl and Nickel, 2007; Kraemer et al., 2017). Sensitivity to lower and higher frequencies increases with age, with responses to 12 kHz appearing as late as 2-3 months after hatching (there are small differences between the American *Tyto furcata* and European *Tyto alba*). Thus, these altricial birds achieve their sensitivity to sound during a prolonged period of development that coincides with the maturation of the skull and facial ruff (Haresign and Moiseff, 1988; Hausmann et al., 2010). The slow maturation of barn owl hearing allowed us to identify a critical period for auditory experience in the nucleus laminaris; we were able to insert an earmold plug when the young owls could hear frequencies up to 1-5 kHz (about 2 weeks after hatching) but were insensitive to sounds of higher frequency, which mature later, at 1-2 month for 8 kHz (Köppl and Nickel, 2007; Kraemer et al., 2017). Since maps of ITD were only shifted in regions of NL with best frequencies above about 5 kHz, this suggests that experience is required for final maturation of the ITD circuit. These findings are consistent with the studies of the development of phase locking in the barn owl's auditory nerve, in which phase locking emerges at about the same time as frequency tuning, and and over a prolonged period of time. There are also strong parallels with results from the work on the gerbil brainstem discussed above, where activity dependent refinement occurs in the first days after hearing onset. Delays in maturation with white noise exposure suggest that not only activity, but patterned activity, is required (Seidl and Grothe, 2005).

Modification of ITD circuits

Our data suggest that the axonal delay-line inputs to NL are plastic within a narrow time window around the onset of normal auditory experience, and furthermore, that the effects of monaural manipulation of acoustic experience appear to be predominantly ipsilateral. We had predicted that an acoustic delay caused by conductive hearing loss in one ear might be compensated for by an advance in neural conduction delay in the inputs to NL. We reasoned that these "faster" inputs could be detected after ear insert removal by a change in the ITD map, as a downward shift of the location of 0µs best ITD in the ipsilateral map, and a matching upward shift on the contralateral side. The results were more complex than predicted. Only those parts of NL that would respond to frequencies that the owl could not hear at the time of plug insertion appeared to be plastic. Furthermore, only the ITD maps in the NL ipsilateral to the manipulated ear changed. One possible explanation for the prominence of ipsilateral changes is that ipsilateral conduction times may be more readily adjusted by shortening axonal projections or thickening myelination, for example. In contrast, speeding up of the contralateral projection from the plugged side might be harder because the contralateral axons are already thicker and faster to compensate the longer

distance than the ipsilateral projection (Seidl ref). Similar ipsilateral effects were observed in the nuclei of the lateral lemniscus on the side ipsilateral to the earplug, in barn owls raised with a unilateral earplug (Mogdans and Knudsen 1992).

Identification of the mechanisms underlying modification of ITD circuits will require future study. Our analyses did not reveal misaligned frequency tuning (Shamma et al., 1989; Pena et al., 2001; Carr et al., 2009; Plauška et al., 2017), which suggest that stereausis does not underlie the shift in best ITD. The effect of side suggests the action of both or either of two mechanisms previously observed in gerbils: altered inhibition and changes in myelination. Gerbils show local and experience dependent change in myelination and conduction velocity of inputs to the superior olive (Lehnert et al., 2014; Ford et al., 2015; Sinclair et al., 2017; Stange-Marten et al., 2017; Dutta et al., 2018), and similar mechanisms may apply to the developing barn owl circuit. For example, myelination in the barn owl NL peaks at the third week posthatch, and myelinating oligodendrocyte density approaches adult levels by one month, when the head reaches its adult width (Cheng and Carr, 2007).

Changes in inhibition could also potentially compensate for the small phase delays measured in the barn owl NL. In mammals, the mammalian medial superior olive receives predominantly glycinergic input from the nucleus of the trapezoid body that acts to shift ITD toward the contralateral hemisphere (Brand et al., 2002; Kapfer et al., 2002; Seidl and Grothe, 2005; Pecka et al., 2008; Franken et al., 2015; Beiderbeck et al., 2018; Winters and Golding, 2018). Similar circuits are found in birds, and NL receives inhibitory input from the ipsilateral superior olive (Carr et al., 1989; Fujita and Konishi, 1991; Burger et al., 2011). Glycine and GABA are co-expressed in avian brainstem auditory nuclei (Kuo et al., 2009; Coleman et al., 2011; Fischl et al., 2014), although neither GABA nor glycine have been implicated in shifts in ITD tuning so far. Instead, inhibition has been linked to the quality of such tuning (Grün et al., 1992; Pena et al., 1996; Nishino et al., 2008). GABAergic inputs act upon both laminaris neurons and on their inputs from the first order nucleus magnocellularis, apparently to maintain dynamic range, and sharpen the coincidence window in laminaris neurons (Grün et al., 1992; Hyson et al., 1995; Pena et al., 1996; Funabiki et al., 1998; Lu et al., 2005; Burger and Rubel, 2008; Nishino et al., 2008; Fukui et al., 2010; Burger et al., 2011; Coleman et al., 2011; Fischl et al., 2012; Yamada et al., 2013; Hamlet et al., 2014; Carroll and Hyson, 2016). In chickens, inputs from local inhibitory GABAergic neurons have also been shown to improve ITD-tuning over a wide range of excitatory levels (Nishino et al., 2008; Yamada et al., 2013). Existing circuits allow for monaural effects; the superior olivary nuclei mutually inhibit each other, at least in the chicken (Burger et al., 2005). Thus, loud sounds in one ear should increase inhibition on the ipsilateral side and decrease inhibition on the contralateral side and potentially alter response latency (Burger et al., 2011).

Acknowledgements

We acknowledge Dr. E. Brittan-Powell for help with calibration and ABR recordings, and Dr. E. Smith for help with equipment and calibration. We thank Dr. Hermann Wagner and Sandra Brill for help measuring the neurophonic and Dr. Sahil Shah for establishing the lesion measurement paradigm. This research was sponsored by National Institute on Deafness and Other Communications Disorders (NIDCD) grant DC-000436 and DC-019341 (CEC). Research at the Carl von Ossietzky University of Oldenburg was supported in part by awards from the Hanse-WissenschaftKolleg, and the Alexander von Humboldt foundation.

Figure legends

Figure 1. ABR evaluation of earmold plugs

A. Average ABR audiograms for free field stimuli, for plug reared (inserts removed) and age matched control adults (n=8, 4 plugged and 4 control). Error bars show standard deviation in dB SPL.

B. Earmold plugs induce reliable sound attenuation. ABR audiograms for 2 P21 animals each, with no plug, a single plug or both ears plugged. Thresholds were higher than with no insert with a single earplug, and highest with two plugs. The adult audiogram from A is shown for comparison (Kraemer et al., 2017). Click thresholds for no plug or a single plug at P21 are shown at 0.1 kHz.

C. Representative ABR traces from a single P21 animal before (blue) and after (grey) acute bilateral ear plug insertion. Traces were evoked by a click stimulus at t=0.

Figure 2. Predicted shift in ITD representation.

A. Schematic connections from the auditory nerve (AN) to the first order nucleus magnocellularis (NM) and to the nucleus laminaris (NL), on right hand side (rhs) of the brainstem, from (Ashida and Carr, 2011).

B. Schematic map of nucleus laminaris (rhs), with delay line axons from NM interdigitating in NL to create the maps of ITD. The dashed red line marks the position of 0µs best ITD. Medial in the brainstem is to the left.

C, D. Diagrams of rhs ITD maps in NL. Blue shading shows locations of best ITDs corresponding to sound sources in the ipsilateral hemifield, red shows contralateral ITDs and the pale diagonal band shows 0µs or frontal ITD, data from (Carr et al., 2015). C. Normal map, also predicted if there is no compensation for the altered auditory experience. D. Predicted shift in ITD representation after insert removal if there were compensation for ipsilateral insert rearing.

Figure 3. Maps of ITD in NL.

A. Exemplar ITD sensitive recordings through lhs (plug side) NL show a shift in best ITD from contralateral to frontal ITDs with recording electrode depth in a dorso-ventral series, as shown by increasing shades of blue (light blue most dorsal recording at 10,100 µm, thick line closest to 0µs best ITD, darkest line most ventral recording at 10,600µm depth). Neurophonic responses in NL were evoked by binaural tones (5.6 kHz) that varied in ITD, and ITD-sensitive responses were recorded only within NL.

B. Exemplar lesions from penetrations through lhs and rhs NL: Lesions mark 0-µs best ITD. Nissl stained transverse 40µm section at the level of central NL. The dorsal (at the top) and ventral (at the bottom) borders of NL are outlined by a glial border that surrounds NL, with the tracts made up of NM axons above and below the borders. There are lesions on both sides in central NL at ITD 0µs, 46% along the tonotopic axis, and 18% up from the ventral edge of NL (lhs, black-ringed symbol in C) and 44% along tonotopic axis and 24% from the ventral edge (rhs, black-center symbol in D). Scale bar=1000µm.

C. Locations of lesions in NL revealed a systematic shift in the mapping of frontal space, around 0 µs best ITD (dashed line shows normal data from (Carr et al., 2015)), in NL ipsilateral to the earmold plug. Each data point marks the dorso-ventral and isofrequency axis coordinates of a 0 µs best ITD recording site. The depth of lesions marking 0 µs best ITD in NL increased with increasingly lateral position along an isofrequency band. Blue symbol colors denote recordings from regions of NL with best frequencies

below 5 kHz, and green symbols recordings above 5 kHz. Note C and D share a common x-axis, marked as % iso-frequency axis. Regression line colors match symbol color.

D. Location of lesions in NL contralateral to the earmold plug. Blue symbol color denotes recordings from regions of NL with best frequencies ≤ 5 kHz, and green symbols recordings > 5 kHz. Note C and D share a common x-axis, marked as % position along iso-frequency band. Regression line colors match symbol color.

Figure 4. Plug effects on the strength of the inputs to NL.

A. Diagram of earmold plug placement in the left ear, with schematic transverse section through the brainstem showing left (plug) ear inputs in red to the nucleus magnocellularis (NM). NM projects to both ipsilateral (red) NL and to the contralateral (magenta) NL. The right hand ear inputs are shown in blue to the right NM. Right NM projects to ipsilateral (blue) NL, and to contralateral (cyan) NL. Color codes are maintained in the figure to faciliate comparisons, and filled symbols show inputs from plug side ear.

B. Exemplar iso-level neurophonic response curves to stimulation of the ipsi (blue) and contralateral (magenta) ear, with SNR (dashed lines) computed from each recording (SNR_{max} of 18.16 for this example). The notation $R_{brain}\,R_{stimulus}$ and $R_{brain}\,L_{stimulus}$ refers to brainstem side of the recordings and stimulus location.

C. SNR_{max} for all BF responses recorded on both left (plug) and right sides of the brain. Responses to stimuli that were ipsilateral to the earmold plug use filled symbols, *(LL, RL*). Responses to stimulation of the right ear use open symbols, *RR, LR.*) Dashed line divides plot by frequency into low (below 5 kHz) and high frequency responses (above 5 kHz).

D. Box plots of the same SNR_{max} data as in C, for both low and high (>5 kHz) best frequency populations, including age-matched controls (grey), on plug (filled symbols) and no plug (open symbols) brain side. Same color code as in A, C. For pairwise comparisons for low best frequency regions, * show LL significantly different to RR, $p<0.005$. For high best frequency regions on NL, * show significantly different control vs. LL ($p<0.0001$), plug LL vs. plug LR ($p<0.001$), plug LL vs. RL ($p<0.018$), and plug LL vs RR ($p<0.0001$).

E. Comparison of estimated marginal means computed from linear mixed model analysis of all neurophonic SNR_{max} data from animals with earmold plugs and age-matched controls revealed that, for recordings with best frequencies ≤5 kHz, SNR_{max} of NL neurophonics evoked by ipsilateral stimulation on the plugged side ("plug ipsi" in lower panel), were significantly different to those evoked by contralateral stimulation on the unplugged side. Confidence intervals for estimated marginal means are indicated by blue bars; pairwise comparisons are shown as red arrows with significant differences between groups indicated by non-overlapping arrows.

Figure 5. ITD responses on both sides of the brain.

A. Mean power spectral density (PSD) of the driven response in B, for recording from the unmanipulated side. PSD based on activity 15–95 ms after the onset of the tone, and shows the PSD at best and worst ITDs. Note the large "signal" peak (0.011 mV^2/kHz) at the stimulus frequency for the favorable ITD (arrow at 6.1 kHz) and the average spectra level around the peak ("noise": 7*10^-5 mV^2/kHz). For the PSD of the response to unfavorable ITD the signal peak height was 11*10^-5 mV^2/kHz and the noise level was 3*10^-5 mV^2/kHz.

B. Exemplar neurophonic ITD curve with best-frequency tones as the stimulus, on the unmanipulated side. Response was obtained from the variance of the sustained activity (onset excluded) ± SE across trials, where 100% corresponds to 0.79 mV^2 in this example (dashed line). The SNR (blue line) is based

on the signal and noise levels of the response PSDs to respective stimulus ITDs, maximum SNR corresponds to 22.4 dB. Stimulation at 50 dB SPL; stimulus frequency 6.1 kHz.

C. Mean PSD of the driven response in D, for recording from the side ipsilateral to the plug; note the large signal peak (0.78 mV^2/kHz) at the stimulus frequency for the favorable ITD (arrow at 5.8 kHz) and the average spectra level around the peak ("noise": 6*10^-4 mV^2/kHz for the favorable ITD). For the PSD of the response to unfavorable ITD the signal peak height was 8*10^-4 mV^2/kHz and the noise level was 3*10^-4 mV^2/kHz.

D. Exemplar neurophonic ITD curve with best-frequency tones as the stimulus in NL contralateral to the plugged ear. Response was obtained from the variance of the sustained activity (onset excluded) ± SE across trials, where 100% corresponds to 6.30 mV^2 in this example (dashed line). The maximum SNR (red line) corresponds to 21.1 dB. Stimulation at 50 dB SPL; stimulus frequency 5.8 kHz.

E. SNR values for all ITD-sensitive neurophonic recordings from animals raised with an earmold plug, separated according to brainstem side relative to the manipulated ear (ipsilateral, red circles and contralateral, blue circles). Age-matched control measures of SNR in NL are also shown (open grey circles). Vertical line marks border between high (>5kHz) and low best frequency regions of NL.

F. Box and whisker plots of all SNR values computed from ITD-sensitive neurophonic responses from animals raised with a monaural earmold plug (plug side and opposite side), and age-matched controls.

G. Comparison of estimated marginal means for the main effects of side and BF-population on SNR_{max}, derived from linear mixed-effects modeling. Confidence intervals for estimated marginal means are represented as blue bars; red arrows indicate pairwise comparisons between groups where overlap of arrows indicates statistical non-significance.

H. Difference (in octaves) in best frequency for neurophonic responses to monaural ipsi- or contralateral stimulation, separately for NL on plug side and side with no plug, for all recordings, with age matched controls. Positive difference corresponds to BF (ipsi) > BF(contra).

H*. Cross-correlation of ipsilateral and contralateral SNR peaks did not predict the difference in best ITD.

Figure 6.

A. Example of a lesion used to identify the location of responses to 0µs best ITD. Nissl-stained top half of rhs brainstem, showing NL, NM, nucleus angularis (NA), and the incoming auditory-nerve tract (N8) . Asterisk marks a lesion near the ventrolateral edge of NL (95% along isofrequency band). Scale bar = 1000 µm.

B. Recorded ITD maps were not different to the normal maps in Carr et al. 2015 (solid line). ANCOVA with a z-test for slopes showed that the slopes were not different (p=0.3). A z-test for slopes yielded a p value of 0.64, thus the y-intercepts for the two ITD maps were not statistically different. Neither were they different to the normal map (p=0.696). Regression for line ipsilateral to the device y=-0.503x+0.57, R^2=0.39. Regression contralateral to device y=-0.343+0.578, R^2=0.08.

Literature cited

Aleksandrov LI, Dmitrieva LP (1992) Development of auditory sensitivity of altricial birds: absolute thresholds of the generation of evoked potentials. Neurosci Behav Physiology 22:132–137.

Anderson S, Skoe E, Chandrasekaran B, Kraus N (2010) Neural timing is linked to speech perception in noise. J Neurosci 30:4922.

Arjmand E, Harris D, Dallos P (1988) Developmental changes in frequency mapping of the gerbil cochlea: Comparison of two cochlear locations. Hearing Res 32:93–96.

Ashida G, Carr CE (2011) Sound localization: Jeffress and beyond. Curr Opin Neurobiol 21:745–751 Available at: https://linkinghub.elsevier.com/retrieve/pii/S0959438811000766.

Babola TA, Li S, Gribizis A, Lee BJ, Issa JB, Wang HC, Crair MC, Bergles DE (2018) Homeostatic Control of Spontaneous Activity in the Developing Auditory System. Neuron 99:511-524.e5 Available at: https://doi.org/10.1016/j.neuron.2018.07.004.

Beatty C Nell (1998) Structural Development of the Mammalian Auditory Pathways. In, pp 315–413 Springer Handbook of Auditory Research. New York, NY: Springer New York. Available at: https://doi.org/10.1007/978-1-4612-2186-9_7.

Beiderbeck B, Myoga MH, Müller NIC, Callan AR, Friauf E, Grothe B, Pecka M (2018) Precisely timed inhibition facilitates action potential firing for spatial coding in the auditory brainstem. Nat Commun 9:1771 Available at: http://www.nature.com/articles/s41467-018-04210-y.

Bergan JF, Knudsen EI (2007) Auditory Map Plasticity in Juvenile and Adult Owls. The Senses: A Comprehensive Reference, Vol 3, Audition:6.

Bolhuis JJ (1991) MECHANISMS OF AVIAN IMPRINTING: A REVIEW. Biol Rev 66:303–345 Available at: https://doi.org/10.1111/j.1469-185X.1991.tb01145.x.

Brainard MS, Knudsen EI (1995) Dynamics of visually guided auditory plasticity in the optic tectum of the barn owl. J Neurophysiol 73:595–614 Available at: http://www.ncbi.nlm.nih.gov/entrez/query.fcgi?cmd=Retrieve&db=PubMed&dopt=Citation&list_uids=7760121.

Brand A, Behrend O, Marquardt T, McAlpine D, Grothe B (2002) Precise inhibition is essential for microsecond interaural time difference coding. Nature 417:543–547 Available at: http://www.nature.com/doifinder/10.1038/417543a.

Brenowitz S, Trussell LO (2001) Maturation of synaptic transmission at end-bulb synapses of the cochlear nucleus. J Neurosci 21:9487–9498 Available at: http://www.jneurosci.org/cgi/content/abstract/21/23/9487.

Brittan-Powell EF, Dooling RJ (2004) Development of auditory sensitivity in budgerigars (Melopsittacus undulatus). JASA 115:3092–3102 Available at: http://link.aip.org/link/JASMAN/v115/i6/p3092/s1&Agg=doi.

Brugge JF (1983) Development of Auditory and Vestibular Systems. Dev Auditory Syst:89–120.

Burger RM, Cramer KS, Pfeiffer JD, Rubel EW (2005) Avian superior olivary nucleus provides divergent inhibitory input to parallel auditory pathways. J Comp Neurol 481:6–18.

Burger RM, Fukui I, Ohmori H, Rubel EW (2011) Inhibition in the balance: binaurally coupled inhibitory feedback in sound localization circuitry. J Neurophysiol 106:4–14 Available at: http://www.ncbi.nlm.nih.gov/pmc/articles/PMC3129726/.

Burger RM, Rubel EW (2008) The Senses: A Comprehensive Reference. In (Dallos, Oertel, eds), pp 613–630 The Senses: A Comprehensive Reference. The Senses: A Comprehensive Reference, Vol 3, Audition.

Butler BE, Lomber SG (2013) Functional and structural changes throughout the auditory system following congenital and early-onset deafness: implications for hearing restoration. Frontiers Syst Neurosci 7:92.

Campenhausen M von, Wagner H (2006) Influence of the facial ruff on the sound-receiving characteristics of the barn owl's ears. J Comp Physiol A 192:1073–1082 Available at: http://link.springer.com/10.1007/s00359-006-0139-0.

Caras ML, Sanes DH (2015) Sustained Perceptual Deficits from Transient Sensory Deprivation. J Neurosci 35:10831–10842 Available at: http://pubmed.gov/26224865.

Carr C, Konishi M (1990) A circuit for detection of interaural time differences in the brain stem of the barn owl. J Neurosci 10:3227–3246 Available at: http://eutils.ncbi.nlm.nih.gov/entrez/eutils/elink.fcgi?dbfrom=pubmed&id=2213141&retmode=ref&cmd=prlinks.

Carr CE, Fujita I, Konishi M (1989) Distribution of GABAergic neurons and terminals in the auditory system of the barn owl. J Comp Neurol 286:190–207.

Carr CE, Shah S, Ashida G, McColgan T, Wagner H, Kuokkanen PT, Kempter R, Köppl C (2013) Maps of ITD in the nucleus laminaris of the barn owl. Adv Exp Med Biol 787:215–222 Available at: http://link.springer.com/chapter/10.1007/978-1-4614-1590-9_24.

Carr CE, Shah S, McColgan T, Ashida G, Kuokkanen PT, Brill S, Kempter R, Wagner H (2015) Maps of interaural delay in the owl's nucleus laminaris. J Neurophys 114:1862–1873 Available at: http://www.physiology.org/doi/10.1152/jn.00644.2015.

Carr CE, Soares D, Smolders JWT, Simon JZ (2009) Detection of interaural time differences in the alligator. J Neurosci 29:7978–7990 Available at: http://eutils.ncbi.nlm.nih.gov/entrez/eutils/elink.fcgi?dbfrom=pubmed&id=19553438&retmode=ref&cmd=prlinks.

Carroll BJ, Hyson RL (2016) A role for inhibition in deafness-induced plasticity of the avian auditory brainstem. Neuroscience 327:10–19.

Chang EH, Kotak VC, Sanes DH (2003) Long-Term Depression of Synaptic Inhibition Is Expressed Postsynaptically in the Developing Auditory System. J Neurophysiol 90:1479–1488.

Cheng S-M, Carr CE (2007) Functional delay of myelination of auditory delay lines in the nucleus laminaris of the barn owl. Dev Neurobiol 67:1957–1974 Available at: http://doi.wiley.com/10.1002/dneu.20541.

Clarkson C, Antunes FM, Rubio ME (2016) Conductive Hearing Loss Has Long-Lasting Structural and Molecular Effects on Presynaptic and Postsynaptic Structures of Auditory Nerve Synapses in the Cochlear Nucleus. J Neurosci 36:10214–10227 Available at: http://www.jneurosci.org/cgi/doi/10.1523/JNEUROSCI.0226-16.2016.

Clause A, Kim G, Sonntag M, Weisz CJC, Vetter DE, Rubsamen R, Kandler K (2014) The precise temporal pattern of prehearing spontaneous activity is necessary for tonotopic map refinement. Neuron 82:822–835 Available at: http://linkinghub.elsevier.com/retrieve/pii/S0896627314002918.

Clements M, Kelly JB (1978) Auditory spatial responses of young guinea pigs (Cavia porcellus) during and after ear blocking. J Comp Physiol Psych 92:34–44.

Coleman WL, Fischl MJ, Weimann SR, Burger RM (2011) GABAergic and glycinergic inhibition modulate monaural auditory response properties in the avian superior olivary nucleus. J Neurophys 105:2405–2420 Available at: http://www.ncbi.nlm.nih.gov/pmc/articles/PMC3094186/.

Crins TTH, Rusu SI, Rodriguez-Contreras A, Borst JGG (2011) Developmental Changes in Short-Term Plasticity at the Rat Calyx of Held Synapse. J Neurosci 31:11706–11717 Available at: http://eutils.ncbi.nlm.nih.gov/entrez/eutils/elink.fcgi?dbfrom=pubmed&id=21832200&retmode=ref&cmd=prlinks.

Dum N (1984) Postnatal development of the auditory evoked brainstem potentials in the guinea pig. Acta oto-laryngologica Available at: http://www.tandfonline.com/doi/abs/10.3109/00016488409130965.

Dutta DJ, Woo DH, Lee PR, Pajevic S, Bukalo O, Huffman WC, Wake H, Basser PJ, SheikhBahaei S, Lazarevic V, Smith JC, Fields RD (2018) Regulation of myelin structure and conduction velocity by perinodal astrocytes. Proc Natl Acad Sci USA 115:11832–11837 Available at: http://www.pnas.org/lookup/doi/10.1073/pnas.1811013115.

Dyke KBV, Lieberman R, Presacco A, Anderson S (2017) Development of Phase Locking and Frequency Representation in the Infant Frequency-Following Response. J Speech Lang Hear Res 60:2740–2751 Available at: http://eutils.ncbi.nlm.nih.gov/entrez/eutils/elink.fcgi?dbfrom=pubmed&id=28832878&retmode=ref&cmd=prlinks.

Fischl MJ, Combs TD, Klug A, Grothe B, Burger RM (2012) Modulation of synaptic input by GABAB receptors improves coincidence detection for computation of sound location. J Physiology 590:3047–3066 Available at: http://www.jphysiol.org/cgi/doi/10.1113/jphysiol.2011.226233.

Fischl MJ, Weimann SR, Kearse MG, Burger RM (2014) Slowly emerging glycinergic transmission enhances inhibition in the sound localization pathway of the avian auditory system. J Neurophys 111:565–572 Available at: http://jn.physiology.org/cgi/doi/10.1152/jn.00640.2013.

Ford MC, Alexandrova O, Cossell L, Stange-Marten A, Sinclair J, Kopp-Scheinpflug C, Pecka M, Attwell D, Grothe B (2015) Tuning of Ranvier node and internode properties in myelinated axons to adjust action potential timing. Nat Commun 6:8073 Available at: http://dx.doi.org/10.1038/ncomms9073.

Franken TP, Roberts MT, Wei L, Golding NL, Joris PX (2015) In vivo coincidence detection in mammalian sound localization generates phase delays. Nat Neurosci 18:444–452 Available at: http://eutils.ncbi.nlm.nih.gov/entrez/eutils/elink.fcgi?dbfrom=pubmed&id=25664914&retmode=ref&cmd=prlinks.

Friauf E, Fischer AU, Fuhr MF (2015) Synaptic plasticity in the auditory system: a review. Cell Tissue Res 361:177–213.

Friauf E, Lohmann C (1999) Development of auditory brainstem circuitry. Activity-dependent and activity-independent processes. Cell Tissue Res 297:187–195 Available at: http://eutils.ncbi.nlm.nih.gov/entrez/eutils/elink.fcgi?dbfrom=pubmed&id=10470488&retmode=ref&cmd=prlinks.

Fujita I, Konishi M (1991) The role of GABAergic inhibition in processing of interaural time difference in the owl's auditory system. J Neurosci 11:722–739.

Fukui I, Burger RM, Ohmori H, Rubel EW (2010) GABAergic inhibition sharpens the frequency tuning and enhances phase locking in chicken nucleus magnocellularis neurons. J Neurosci 30:12075–12083 Available at: http://www.jneurosci.org/cgi/doi/10.1523/JNEUROSCI.1484-10.2010.

Funabiki K, Koyano K, Ohmori H (1998) The role of GABAergic inputs for coincidence detection in the neurones of nucleus laminaris of the chick. J Physiol 508 (Pt 3):851–869 Available at: http://doi.wiley.com/10.1111/j.1469-7793.1998.851bp.x.

Gans E, Willis K, Bierman H, Carr C (2012) The interaural canal of the barn owl, Tyto alba. In: Integrative and Comparative Biology (ICB), pp e202–e356 Integrative and Comparative Biology. INTEGRATIVE. Available at: http://scholar.google.com#.

Gold JI, Knudsen EI (1999) Hearing impairment induces frequency-specific adjustments in auditory spatial tuning in the optic tectum of young owls. J Neurophys 82:2197–2209 Available at: http://pubmed.gov/10561399.

Gold JI, Knudsen EI (2000a) A site of auditory experience-dependent plasticity in the neural representation of auditory space in the barn owl's inferior colliculus. J Neurosci 20:3469–3486 Available at: http://eutils.ncbi.nlm.nih.gov/entrez/eutils/elink.fcgi?dbfrom=pubmed&id=10777810&retmode=ref&cmd=prlinks.

Gold JI, Knudsen EI (2000b) Abnormal auditory experience induces frequency-specific adjustments in unit tuning for binaural localization cues in the optic tectum of juvenile owls. J Neurosci 20:862–877 Available at: http://pubmed.gov/10632616.

Gray L, Rubel EW (1985) Development of absolute thresholds in chickens. JASA 77:1162–1172 Available at: http://eutils.ncbi.nlm.nih.gov/entrez/eutils/elink.fcgi?dbfrom=pubmed&id=3980868&retmode=ref&cmd=prlinks.

Grün S, Wagner H, Carr CE, Aersten A (1992) Binaural interaction in the nucleus laminaris of the barn owl: a quantitative model. BrainWorks 1991-0 Available at: http://www.google.com/search?client=safari&rls=en-us&q=Binaural+interaction+in+the+nucleus+laminaris+of+the+barn+owl:+a+quantitative+model&ie=UTF-8&oe=UTF-8.

Hamlet WR, Liu Y-W, Tang Z-Q, Lu Y (2014) Interplay between low threshold voltage-gated K(+) channels and synaptic inhibition in neurons of the chicken nucleus laminaris along its frequency axis. Front Neural Circuits 8:51 Available at: http://journal.frontiersin.org/article/10.3389/fncir.2014.00051/abstract.

Haresign T, Moiseff A (1988) Early Growth and Development of the Common Barn-Owl's Facial Ruff. Auk 105:699–705 Available at: http://www.google.com/search?client=safari&rls=en-us&q=Early+growth+and+development+of+the+common+barn-owl's+facial+ruff&ie=UTF-8&oe=UTF-8.

Hausmann L, Campenhausen M von, Wagner H (2010) Properties of low-frequency head-related transfer functions in the barn owl (Tyto alba). J Comp Physiol A 196:601–612 Available at: http://www.springerlink.com/index/10.1007/s00359-010-0546-0.

Hyson RL, Reyes AD, Rubel EW (1995) A depolarizing inhibitory response to GABA in brainstem auditory neurons of the chick. Brain Research Available at: http://linkinghub.elsevier.com/retrieve/pii/000689939500130I.

Jones SM, Jones TA (1995) The tonotopic map in the embryonic chicken cochlea. Hearing Research Available at: http://linkinghub.elsevier.com/retrieve/pii/037859559400173N.

Jones TA, Jones SM, Paggett K (2001) Primordial rhythmic bursting in embryonic cochlear ganglion cells. J Neurosci 21:8129–8135 Available at: http://www.ncbi.nlm.nih.gov/entrez/query.fcgi?cmd=Retrieve&db=PubMed&dopt=Citation&list_uids=11588185.

Kandler K, Clause A, Noh J (2009) Tonotopic reorganization of developing auditory brainstem circuits. Nature 12:711–717 Available at: http://eutils.ncbi.nlm.nih.gov/entrez/eutils/elink.fcgi?dbfrom=pubmed&id=19471270&retmode=ref&cmd=prlinks.

Kandler K, Gillespie DC (2005) Developmental refinement of inhibitory sound-localization circuits. TINS 28:290–296.

Kapfer C, Seidl AH, Schweizer H, Grothe B (2002) Experience-dependent refinement of inhibitory inputs to auditory coincidence-detector neurons. Nat Neurosci 5:247–253.

Keating P, King AJ (2013) Developmental plasticity of spatial hearing following asymmetric hearing loss: context-dependent cue integration and its clinical implications. Front Syn Neurosci 7:123 Available at: http://journal.frontiersin.org/article/10.3389/fnsys.2013.00123/abstract.

Keller CH, Takahashi TT (1996) Responses to simulated echoes by neurons in the barn owl's auditory space map. J Comp Physiol A 178:499–512 Available at: http://www.google.com/search?client=safari&rls=en-us&q=Responses+to+simulated+echoes+by+neurons+in+the+barn+owl's+auditory+space+map&ie=UTF-8&oe=UTF-8.

Kettler L, Christensen-Dalsgaard J, Larsen ON, Wagner H (2016) Low frequency eardrum directionality in the barn owl induced by sound transmission through the interaural canal. Biol Cybern:1–11 Available at: http://link.springer.com/10.1007/s00422-016-0689-3.

Keuroghlian AS, Knudsen EI (2007) Adaptive auditory plasticity in developing and adult animals. Prog Neurobiol 82:109–121 Available at: http://www.sciencedirect.com/science?_ob=ArticleURL&_udi=B6T0R-4NFH0F3-1&_user=961305&_rdoc=1&_fmt=&_orig=search&_sort=d&view=c&_version=1&_urlVersion=0&_userid=961305&md5=c2a18820950b0d4763a723bdd1ca5418.

King AJ, Parsons CH, Moore DR (2000) Plasticity in the neural coding of auditory space in the mammalian brain. Proc National Acad Sci 97:11821–11828 Available at: http://www.pnas.org/cgi/doi/10.1073/pnas.97.22.11821.

Klug A, Borst JGG, Carlson BA, Kopp-Scheinpflug C, Klyachko VA, Xu-Friedman MA (2012) How do short-term changes at synapses fine-tune information processing? J Neurosci 32:14058–14063 Available at: http://eutils.ncbi.nlm.nih.gov/entrez/eutils/elink.fcgi?dbfrom=pubmed&id=23055473&retmode=ref&cmd=prlinks.

Knudsen EI (2002) Instructed learning in the auditory localization pathway of the barn owl. Nature 417:322–328 Available at: http://neurosci.info/courses/systems/CentralPlas/knudsen02.pdf.

Knudsen EI, Brainard M (1995) Creating a unified representation of visual and auditory space in the brain. Annu Rev Neurosci 18:19–43 Available at: http://www.annualreviews.org/doi/10.1146/annurev.ne.18.030195.000315.

Knudsen EI, Knudsen PF, Esterly SD (1984) A critical period for the recovery of sound localization accuracy following monaural occlusion in the barn owl. J Neurosci 4:1012–1020 Available at: http://www.ncbi.nlm.nih.gov/entrez/query.fcgi?cmd=Retrieve&db=PubMed&dopt=Citation&list_uids=6716128.

Köppl C (1997) Frequency tuning and spontaneous activity in the auditory nerve and cochlear nucleus magnocellularis of the barn owl Tyto alba. J Neurophys 77:364–377 Available at: http://eutils.ncbi.nlm.nih.gov/entrez/eutils/elink.fcgi?dbfrom=pubmed&id=9120577&retmode=ref&cmd=prlinks.

Köppl C (2001) Tonotopic projections of the auditory nerve to the cochlear nucleus angularis in the barn owl. JARO 2:41–53.

Köppl C (2007) Development of Phase Locking in the Barn Owl's Auditory Nerve: The Emergence of Extreme Temporal Precision. ARO abstract.

Köppl C, Ashida G, Brill S, Kempter R, Wagner H (2012) Experience-dependent plasticity in the nucleus laminaris of the barn owl. frontiersin.org Available at: http://www.frontiersin.org/10.3389/conf.fnbeh.2012.27.00396/event_abstract.

Köppl C, Futterer E, Nieder B, Sistermann R, Wagner H (2005) Embryonic and posthatching development of the barn owl (Tyto alba): reference data for age determination. Dev Dyn 233:1248–1260 Available at: http://www3.interscience.wiley.com/cgi-bin/abstract/110482413/ABSTRACT?CRETRY=1&SRETRY=0.

Köppl C, Nickel R (2007) Prolonged maturation of cochlear function in the barn owl after hatching. J Comp physiol 193:613–624 Available at: http://link.springer.com/10.1007/s00359-007-0216-z.

Kohrman DC, Borges BC, Cassinotti LR, Ji L, Corfas G (2021) Axon–glia interactions in the ascending auditory system. Dev Neurobiol 81:546–567.

Konishi M (1973) Development of auditory neuronal responses in avian embryos. Proc Natl Acad Sci USA 70:1795–1798.

Kraemer A, Baxter C, Hendrix A, Carr CE (2017) Development of auditory sensitivity in the barn owl. J Comp Physiol A 203:843–853 Available at: http://link.springer.com/10.1007/s00359-017-1197-1.

Kral A, Hubka P, Heid S, Tillein J (2013) Single-sided deafness leads to unilateral aural preference within an early sensitive period. Brain 136:180–193 Available at: http://eutils.ncbi.nlm.nih.gov/entrez/eutils/elink.fcgi?dbfrom=pubmed&id=23233722&retmode=ref&cmd=prlinks.

Kubke MF, Carr C (2006) Development of the auditory centers responsible for sound localization. In: Springer Handbook of Auditory Research (Popper AN, Fay RR, eds), pp 179–237. Sound Source Localization. Available at: https://link.springer.com/chapter/10.1007/0-387-28863-5_6.

Kubke MF, Carr CE (2000) Development of the auditory brainstem of birds: comparison between barn owls and chickens. Hearing Research 147:1–20 Available at: https://linkinghub.elsevier.com/retrieve/pii/S0378595500001167.

Kumpik DP, King AJ (2019) A review of the effects of unilateral hearing loss on spatial hearing. Hearing Research 372:17–28 Available at: https://doi.org/10.1016/j.heares.2018.08.003.

Kuo SP, Bradley LA, Trussell LO (2009) Heterogeneous Kinetics and Pharmacology of Synaptic Inhibition in the Chick Auditory Brainstem. J Neurosci 29:9625–9634 Available at: http://www.jneurosci.org/cgi/doi/10.1523/JNEUROSCI.0103-09.2009.

Kuokkanen PT, Ashida G, Carr CE, Wagner H, Kempter R (2013) Linear summation in the barn owl's brainstem underlies responses to interaural time differences. J Neurophys 110:117–130 Available at: http://www.ncbi.nlm.nih.gov/pmc/articles/PMC3727037/.

Kuokkanen PT, Ashida G, Kraemer A, McColgan T, Funabiki K, Wagner H, Köppl C, Carr CE, Kempter R (2018) Contribution of action potentials to the extracellular field potential in the nucleus laminaris of barn owl. J Neurophys 119:1422–1436 Available at: http://pubmed.gov/29357463.

Kuokkanen PT, Wagner H, Ashida G, Carr CE, Kempter R (2010) On the origin of the extracellular field potential in the nucleus laminaris of the barn owl (Tyto alba). J Neurophys 104:2274–2290 Available at: http://jn.physiology.org/cgi/doi/10.1152/jn.00395.2010.

Lauer AM, Dent ML, Sun W, Xu-Friedman MA (2019) Effects of non-traumatic noise and conductive hearing loss on auditory system function. Neuroscience 407:182–191.

Lehnert S, Ford MC, Alexandrova O, Hellmundt F, Felmy F, Grothe B, Leibold C (2014) Action potential generation in an anatomically constrained model of medial superior olive axons. J Neurosci 34:5370–5384 Available at: http://eutils.ncbi.nlm.nih.gov/entrez/eutils/elink.fcgi?dbfrom=pubmed&id=24719114&retmode=ref&cmd=prlinks.

Lu Y, Burger RM, Rubel EW (2005) GABA(B) receptor activation modulates GABA(A) receptor-mediated inhibition in chicken nucleus magnocellularis neurons. J Neurophys 93:1429–1438 Available at: http://eutils.ncbi.nlm.nih.gov/entrez/eutils/elink.fcgi?dbfrom=pubmed&id=15483063&retmode=ref&cmd=prlinks.

MacLeod KM, Carr CE (2012) Synaptic mechanisms of coincidence detection. In (Trussell LO, Popper AN, eds), pp 135–164 Synaptic Mechanisms in the Auditory System. Synaptic Mechanisms in the Auditory System. Available at: http://link.springer.com/chapter/10.1007/978-1-4419-9517-9_6.

Magnusson AK, Kapfer C, Grothe B, Koch U (2005) Maturation of glycinergic inhibition in the gerbil medial superior olive after hearing onset. J Physiology 568:497–512 Available at: http://doi.wiley.com/10.1113/jphysiol.2005.094763.

Maier JK, Kindermann T, Grothe B, Klump GM (2008) Effects of omni-directional noise-exposure during hearing onset and age on auditory spatial resolution in the Mongolian gerbil (Meriones unguiculatus) — a behavioral approach. Brain Res 1220:47–57.

Manley GA, Köppl C, Konishi M (1988) A neural map of interaural intensity differences in the brain stem of the barn owl. J Neurosci 8:2665–2676 Available at: http://pubmed.gov/3411346.

Mann ZF, Kelley MW (2011) Development of tonotopy in the auditory periphery. Hearing Research 276:2–15 Available at: http://linkinghub.elsevier.com/retrieve/pii/S0378595511000141.

McColgan T, Shah S, Köppl C, Carr C, Wagner H (2014) A functional circuit model of interaural time difference processing. J Neurophysiol 112:2850–2864 Available at: http://eutils.ncbi.nlm.nih.gov/entrez/eutils/elink.fcgi?dbfrom=pubmed&id=25185809&retmode=ref&cmd=prlinks.

McFadden SL, Walsh EJ, McGee J (1996) Onset and development of auditory brainstem responses in the Mongolian gerbil (Meriones unguiculatus). Hearing Research 100:68–79 Available at: https://linkinghub.elsevier.com/retrieve/pii/0378595596001086.

Miller GL, Knudsen EI (2003) Adaptive plasticity in the auditory thalamus of juvenile barn owls. J Neurosci 23:1059–1065 Available at: http://www.ncbi.nlm.nih.gov/entrez/query.fcgi?cmd=Retrieve&db=PubMed&dopt=Citation&list_uids=12574436.

Mogdans J, Knudsen EI (1992) Adaptive adjustment of unit tuning to sound localization cues in response to monaural occlusion in developing owl optic tectum. J Neurosci 12:3473–3484 Available at: http://eutils.ncbi.nlm.nih.gov/entrez/eutils/elink.fcgi?dbfrom=pubmed&id=1527591&retmode=ref&cmd=prlinks.

Mogdans J, Knudsen EI (1993) Early monaural occlusion alters the neural map of interaural level differences in the inferior colliculus of the barn owl. Brain Research 619:29–38 Available at: https://linkinghub.elsevier.com/retrieve/pii/000689939391593H.

Mogdans J, Knudsen EI (1994) Site of auditory plasticity in the brain stem (VLVp) of the owl revealed by early monaural occlusion. J Neurophys Available at: http://jn.physiology.org/cgi/content/abstract/72/6/2875.

Moore DR (1982) Late onset of hearing in the ferret. Brain Res 253:309–311.

Moore DR (2009) Postnatal Development of the Mammalian Central Auditory System and the Neural Consequences of Auditory Deprivation. Acta Oto-laryngol 99:19–30.

Moore DR, Hine JE, Jiang ZD, Matsuda H, Parsons CH, King AJ (1999) Conductive Hearing Loss Produces a Reversible Binaural Hearing Impairment. J Neurosci 19:8704–8711 Available at: http://www.ncbi.nlm.nih.gov/entrez/query.fcgi?cmd=Retrieve&db=PubMed&dopt=Citation&list_uids=10493771.

Moore DR, King AJ (2004) Plasticity of Binaural Systems. In: Plasticity of the Auditory System (Parks, Rubel, Popper EW, Fay, eds), pp 96–172 Springer Handbook of Auditory Research. Available at: http://www.google.de/search?client=safari&rls=en-us&q=Plasticity+of+binaural+systems&ie=UTF-8&oe=UTF-8&redir_esc=&ei=iiawT8OcOMXMtAaluoDABg.

Mowery TM, Kotak VC, Sanes DH (2015) Transient Hearing Loss Within a Critical Period Causes Persistent Changes to Cellular Properties in Adult Auditory Cortex. Cerebral Cortex 25:2083–2094 Available at: https://academic.oup.com/cercor/article-lookup/doi/10.1093/cercor/bhu013.

Ngodup T, Goetz JA, McGuire BC, Sun W, Lauer AM, Xu-Friedman MA (2015) Activity-dependent, homeostatic regulation of neurotransmitter release from auditory nerve fibers. Proc Natl Acad Sci USA:201420885 Available at: http://www.pnas.org/lookup/doi/10.1073/pnas.1420885112.

Nishino E, Yamada R, Kuba H, Hioki H, Furuta T, Kaneko T, Ohmori H (2008) Sound-Intensity-Dependent Compensation for the Small Interaural Time Difference Cue for Sound Source Localization. J Neurosci 28:7153–7164 Available at: http://www.jneurosci.org/cgi/doi/10.1523/JNEUROSCI.4398-07.2008.

Parks TN, Rubel EW, Popper AN, Fay RR (2004) Plasticity of the auditory system. New York : Springer. Available at: http://lccn.loc.gov/2004041730.

Pecka M, Brand A, Behrend O, Grothe B (2008) Interaural time difference processing in the mammalian medial superior olive: the role of glycinergic inhibition. J Neurosci 28:6914–6925 Available at: http://www.jneurosci.org/cgi/doi/10.1523/JNEUROSCI.1660-08.2008.

Pena JL, Viete S, Albeck Y, Konishi M (1996) Tolerance to sound intensity of binaural coincidence detection in the nucleus laminaris of the owl. J Neurosci 16:7046–7054 Available at: http://pubmed.gov/8824340.

Pena JL, Viete S, Funabiki K, Saberi K, Konishi M (2001) Cochlear and neural delays for coincidence detection in owls. J Neurosci 21:9455–9459 Available at: http://eutils.ncbi.nlm.nih.gov/entrez/eutils/elink.fcgi?dbfrom=pubmed&id=11717379&retmode=ref&cmd=prlinks.

Persic D, Thomas ME, Pelekanos V, Ryugo DK, Takesian AE, Krumbholz K, Pyott SJ (2020) Regulation of auditory plasticity during critical periods and following hearing loss. Hearing Res 397:107976.

Plauška A, Heijden M van der, Borst JGG (2017) A Test of the Stereausis Hypothesis for Sound Localization in Mammals. J Neurosci 37:7278–7289.

Poganiatz I, Wagner H (2001) Sound-localization experiments with barn owls in virtual space: influence of broadband interaural level different on head-turning behavior. J Comp Physiol A 187:225–233 Available at: http://www.ncbi.nlm.nih.gov/entrez/query.fcgi?cmd=Retrieve&db=PubMed&dopt=Citation&list_uids=11401202 .

Polley DB, Thompson JH, Guo W (2013) Brief hearing loss disrupts binaural integration during two early critical periods of auditory cortex development. Nat Commun 4:2547 Available at: http://www.nature.com/articles/ncomms3547.

Popescu MV, Polley DB (2010) Monaural Deprivation Disrupts Development of Binaural Selectivity in Auditory Midbrain and Cortex. Neuron 65:718–731 Available at: http://dx.doi.org/10.1016/j.neuron.2010.02.019.

Pujol R, Hilding D (1973) Anatomy And Physiology Of The Onset Of Auditory Function. Acta Oto-laryngol 76:1–10 Available at: https://doi.org/10.3109/00016487309121476.

Razak KA, Fuzessery ZM (2007) Development of Inhibitory Mechanisms Underlying Selectivity for the Rate and Direction of Frequency-Modulated Sweeps in the Auditory Cortex. J Neurosci 27:1769–1781.

Rich V, Carr CE (1999) Husbandry and captive rearing of barn owls. Poul Av Bio Rev 10:91–95 Available at: https://academic.oup.com/condor/article/116/4/507-517/5153123.

Rivera M, Louder MIM, Kleindorfer S, Liu W, Hauber ME (2018) Avian prenatal auditory stimulation: progress and perspectives. Behav Ecol Sociobiol 72:112.

Romand R (1979) Development of auditory nerve activity in kittens. Brain Research 173:554–556.

Rosen MJ, Sarro EC, Kelly JB, Sanes DH (2012) Diminished Behavioral and Neural Sensitivity to Sound Modulation Is Associated with Moderate Developmental Hearing Loss. Plos One 7:e41514.

Rubel EW, Parks TN, Edelman G, WE G, Cowan WM (1988) Organization and development of the avian brainstem auditory system. Auditory Function: Neurobiological Bases of Hearing.

Rubio ME (2020) Auditory brainstem development and plasticity. Curr Opin Physiology 18:7–10.

Sanes D (1993) The development of synaptic function and integration in the central auditory system. J Neurosci 13:2627–2637.

Sanes DH (2002) Right place at the right time. Nat Neurosci 5:187–188.

Sanes DH, Bao S (2009) Tuning up the developing auditory CNS. Curr Opin Neurobiol 19 Available at: http://pubmed.gov/19535241.

Sarro EC, Sanes DH (2010) Prolonged maturation of auditory perception and learning in gerbils. Dev Neurobiol 70:636–648 Available at: http://eutils.ncbi.nlm.nih.gov/entrez/eutils/elink.fcgi?dbfrom=pubmed&id=20506133&retmode=ref&cmd=prlinks.

Sato K, Momose-Sato Y (2003) Optical detection of developmental origin of synaptic function in the embryonic chick vestibulocochlear nuclei. J Neurophys 89:3215–3224 Available at: http://jn.physiology.org/cgi/doi/10.1152/jn.01169.2002.

Saunders JC, Coles RB, Gates GR (1973) The development of auditory evoked responses in the cochlea and cochlear nuclei of the chick. Brain Research 63:59–74 Available at: http://linkinghub.elsevier.com/retrieve/pii/0006899373900760.

Seidl AH, Grothe B (2005) Development of sound localization mechanisms in the mongolian gerbil is shaped by early acoustic experience. J Neurophys 94:1028–1036 Available at: http://www.ncbi.nlm.nih.gov/entrez/query.fcgi?cmd=Retrieve&db=PubMed&dopt=Citation&list_uids=15829592.

Shamma SA, Shen NM, P PG (1989) Stereausis: binaural processing without neural delays. JASA 86:989–1006 Available at: http://eutils.ncbi.nlm.nih.gov/entrez/eutils/elink.fcgi?dbfrom=pubmed&id=2794252&retmode=ref&cmd=prlinks.

Sinclair JL, Fischl MJ, Alexandrova O, Heβ M, Grothe B, Leibold C, Kopp-Scheinpflug C (2017) Sound-Evoked Activity Influences Myelination of Brainstem Axons in the Trapezoid Body. J Neurosci 37:8239–8255 Available at: http://pubmed.gov/28760859.

Sonntag M, Englitz B, Kopp-Scheinpflug C, Rubsamen R (2009) Early Postnatal Development of Spontaneous and Acoustically Evoked Discharge Activity of Principal Cells of the Medial Nucleus of the Trapezoid Body: An In Vivo Study in Mice. J Neurosci 29:9510–9520.

Stange-Marten A, Nabel AL, Sinclair JL, Fischl M, Alexandrova O, Wohlfrom H, Kopp-Scheinpflug C, Pecka M, Grothe B (2017) Input timing for spatial processing is precisely tuned via constant synaptic delays and myelination patterns in the auditory brainstem. Proc National Acad Sci 114:E4851–E4858.

Sullivan WE, Konishi M (1986) Neural map of interaural phase difference in the owl's brainstem. Proc National Acad Sci 83:8400–8404 Available at: http://www.google.com/search?client=safari&rls=en-us&q=Neural+map+of+interaural+phase+difference+in+the+owl's+brainstem&ie=UTF-8&oe=UTF-8.

Takahashi TT, Konishi M (1988) Projections of the cochlear nuclei and nucleus laminaris to the inferior colliculus of the barn owl. J Comp Neurol 274:190–211 Available at: http://eutils.ncbi.nlm.nih.gov/entrez/eutils/elink.fcgi?dbfrom=pubmed&id=2463286&retmode=ref&cmd=prlinks.

Trussell LO (1999) Synaptic mechanisms for coding timing in auditory neurons. Annu Rev Physiol 61:477–496.

Tucci DL, Rubel EW (1985) Afferent influences on brain stem auditory nuclei of the chicken: Effects of conductive and sensorineural hearing loss on N. Magnocellularis. J Comp Neurol 238:371–381 Available at: http://doi.wiley.com/10.1002/cne.902380402.

Tzounopoulos T, Kraus N (2009) Learning to Encode Timing: Mechanisms of Plasticity in the Auditory Brainstem. Neuron 62:463–469 Available at: http://dx.doi.org/10.1016/j.neuron.2009.05.002.

Wagner H, Brill S, Kempter R, Carr CE (2005) Microsecond precision of phase delay in the auditory system of the barn owl. J Neurophys 94:1655–1658 Available at: http://jn.physiology.org/cgi/doi/10.1152/jn.01226.2004.

Wagner H, Brill S, Kempter R, Carr CE (2009) Auditory responses in the barn owl's nucleus laminaris to clicks: impulse response and signal analysis of neurophonic potential. J Neurophys 102:1227–1240 Available at: http://www.ncbi.nlm.nih.gov/pmc/articles/PMC2724332/.

Walsh EJ, McGee J, Javel E (1986a) Development of auditory-evoked potentials in the cat. II. Wave latencies. JASA 79:725–744 Available at: http://scitation.aip.org/content/asa/journal/jasa/79/3/10.1121/1.393462.

Walsh EJ, McGee J, Javel E (1986b) Development of auditory-evoked potentials in the cat. III. Wave amplitudes. JASA 79:745–754 Available at: http://pubmed.gov/3007596.

Werner L (2007) Human Auditory Development. The Senses: A Comprehensive Reference, Vol 3, Audition:24.

Werthat F, Alexandrova O, Grothe B, Koch U (2008) Experience-dependent refinement of the inhibitory axons projecting to the medial superior olive. Dev Neurobiol 68:1454–1462 Available at: http://doi.wiley.com/10.1002/dneu.20660.

Wess JM, Isaiah A, Watkins PV, Kanold PO (2017) Subplate neurons are the first cortical neurons to respond to sensory stimuli. Proc Natl Acad Sci USA 114:12602–12607 Available at: http://www.pnas.org/lookup/doi/10.1073/pnas.1710793114.

Winters BD, Golding NL (2018) Glycinergic Inhibitory Plasticity in Binaural Neurons Is Cumulative and Gated by Developmental Changes in Action Potential Backpropagation. Neuron 98:166-178.e2 Available at: http://linkinghub.elsevier.com/retrieve/pii/S0896627318301788.

Yamada R, Okuda H, Kuba H, Nishino E, Ishii TM, Ohmori H (2013) The Cooperation of Sustained and Phasic Inhibitions Increases the Contrast of ITD-Tuning in Low-Frequency Neurons of the Chick Nucleus Laminaris. J Neurosci 33:3927–3938 Available at: http://www.jneurosci.org/cgi/doi/10.1523/JNEUROSCI.2377-12.2013.

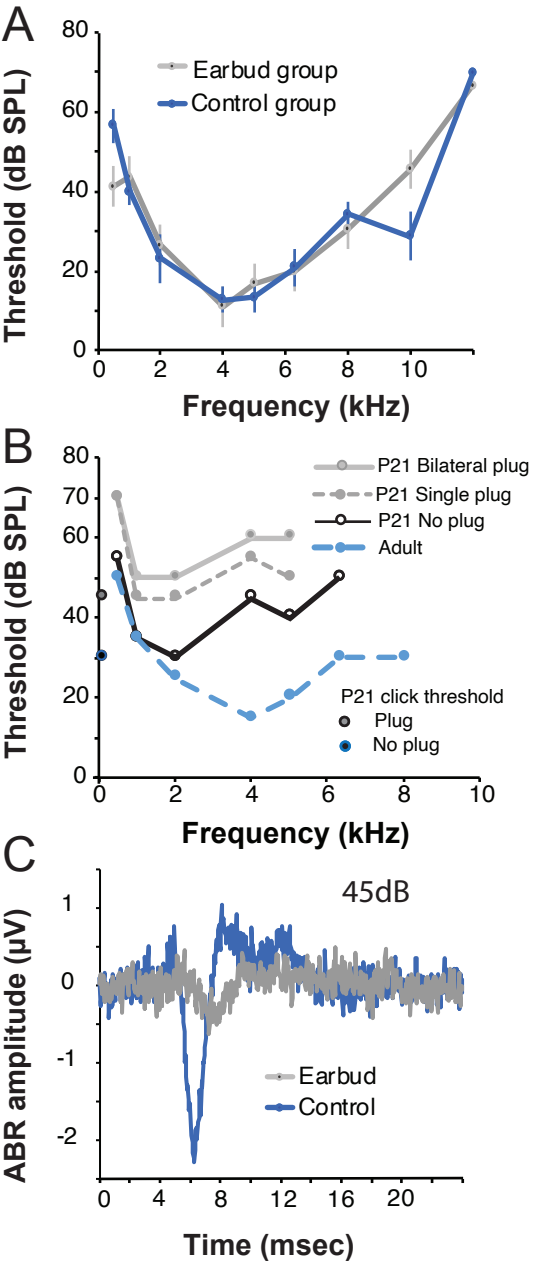
A
Threshold (dB SPL)
Earbud group
Control group
Frequency (kHz)
B
Threshold (dB SPL)
P21 Bilateral plug
P21 Single plug
P21 No plug
Adult
P21 click threshold
Plug
No plug
Frequency (kHz)
C
45dB
ABR amplitude (µV)
Earbud
Control
Time (msec)

Figure 1

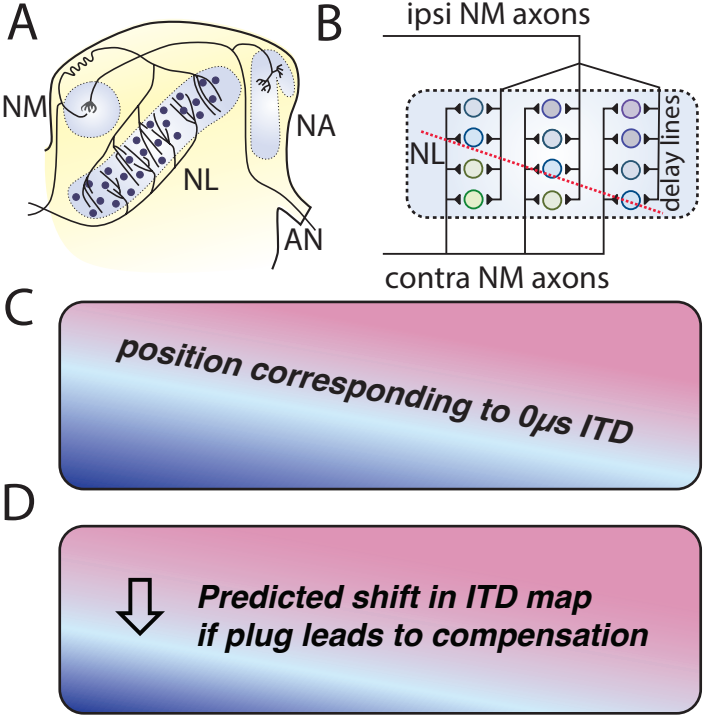
A
NM
NA
NL
AN
B
ipsi NM axons
NL
delay lines
contra NM axons
C
position corresponding to 0μs ITD
D
Predicted shift in ITD map
if plug leads to compensation

Figure 2

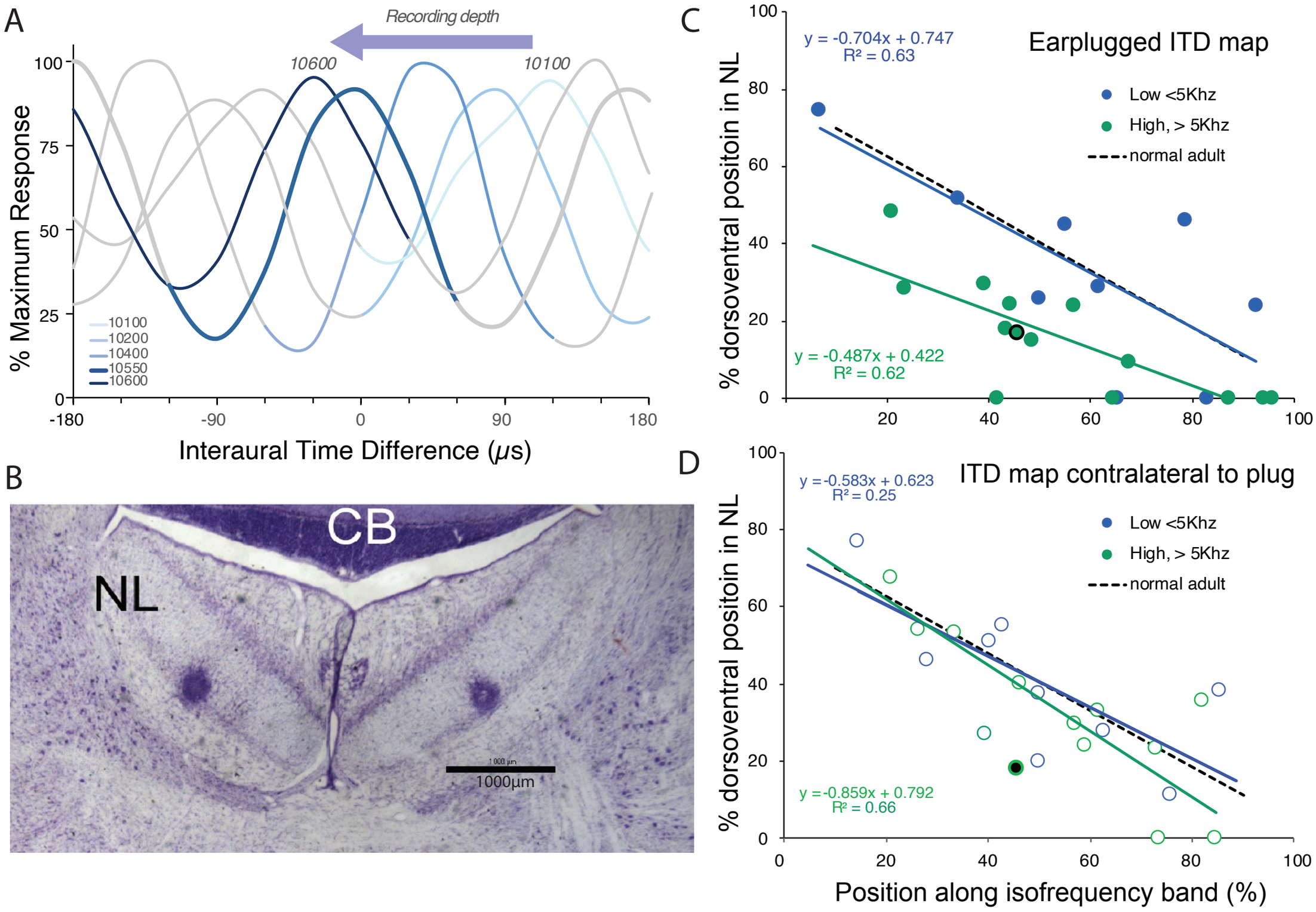
A
Recording depth
10600
10100
% Maximum Response
100
75
50
25
0
10100
10200
10400
10550
10600
-180
-90
0
90
180
Interaural Time Difference (μs)
B
CB
NL
1000µm
C
Earplugged ITD map
y = -0.704x + 0.747
R² = 0.63
Low <5Khz
High, > 5Khz
normal adult
y = -0.487x + 0.422
R² = 0.62
% dorsoventral positoin in NL
D
ITD map contralateral to plug
y = -0.583x + 0.623
R² = 0.25
y = -0.859x + 0.792
R² = 0.66
Position along isofrequency band (%)

Figure 3

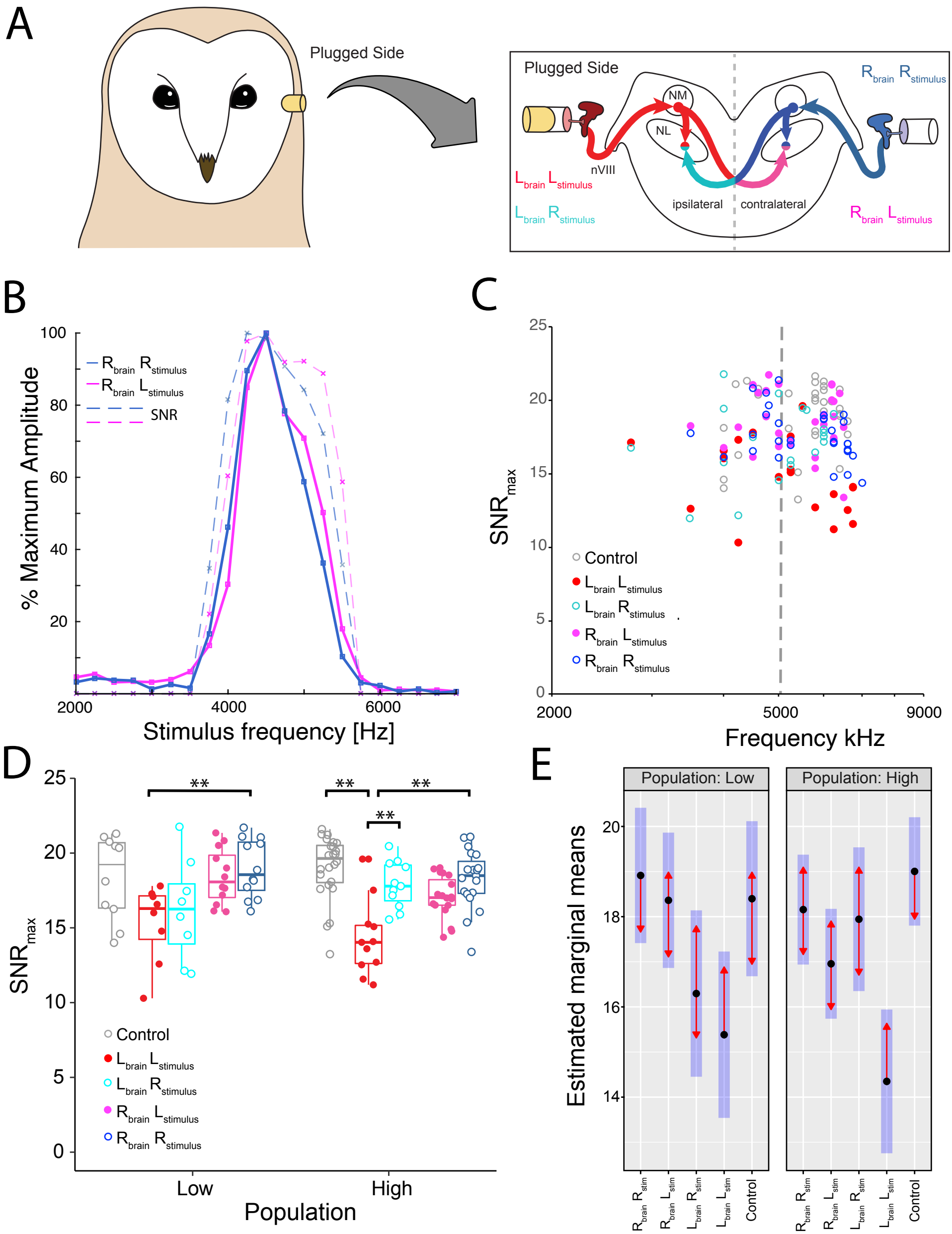
A
Plugged Side
Plugged Side
NM
NL
nVIII
ipsilateral
contralateral
L_{brain} $L_{stimulus}$
L_{brain} $R_{stimulus}$
R_{brain} $R_{stimulus}$
R_{brain} $L_{stimulus}$
B
% Maximum Amplitude
R_{brain} $R_{stimulus}$
R_{brain} $L_{stimulus}$
SNR
Stimulus frequency [Hz]
C
SNR_{max}
Control
L_{brain} $L_{stimulus}$
L_{brain} $R_{stimulus}$
R_{brain} $L_{stimulus}$
R_{brain} $R_{stimulus}$
Frequency kHz
D
SNR_{max}
Control
L_{brain} $L_{stimulus}$
L_{brain} $R_{stimulus}$
R_{brain} $L_{stimulus}$
R_{brain} $R_{stimulus}$
Low
High
Population
E
Population: Low
Population: High
Estimated marginal means
R_{brain} R_{stim}
R_{brain} L_{stim}
L_{brain} R_{stim}
L_{brain} L_{stim}
Control

Figure 4

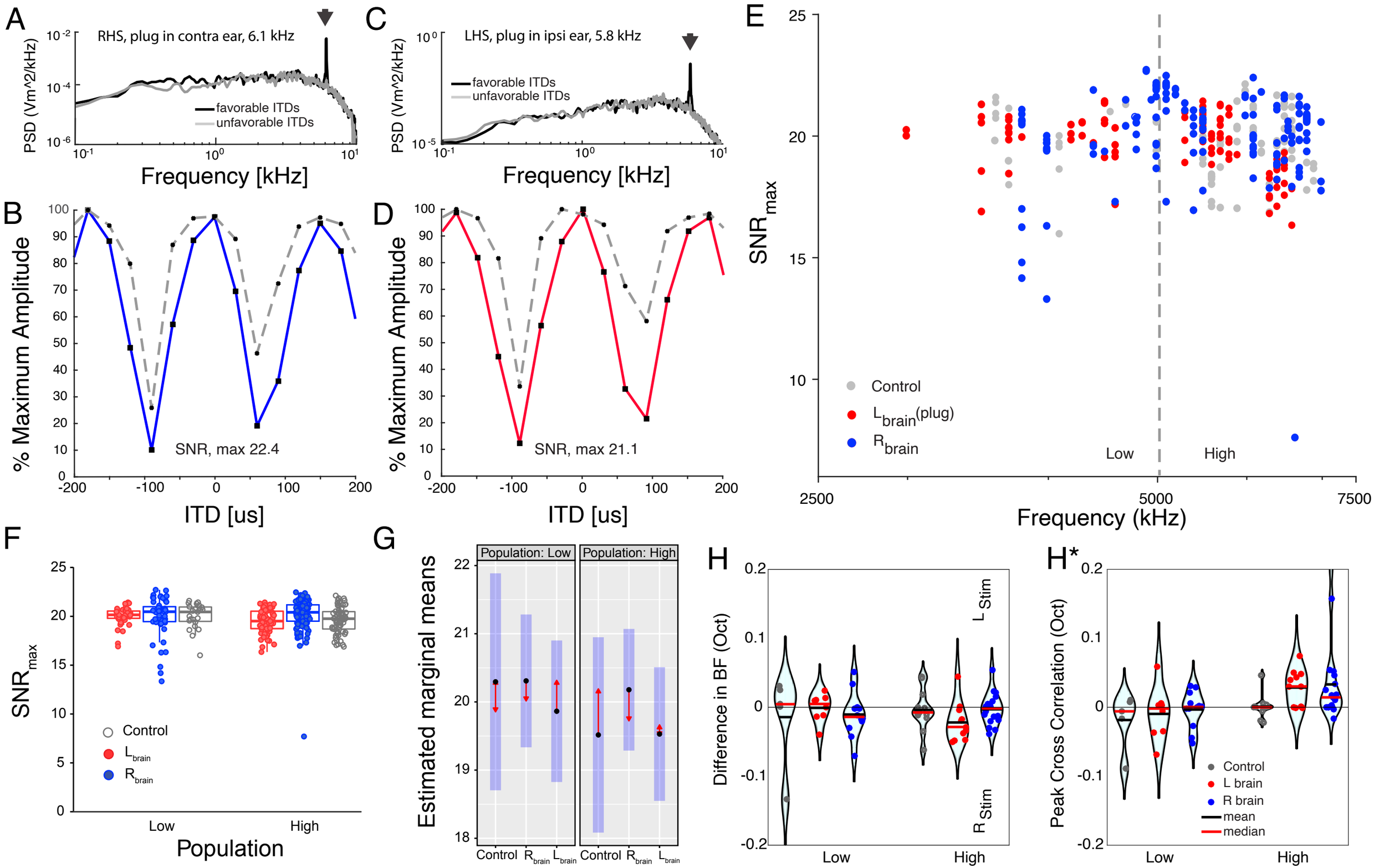
A
RHS, plug in contra ear, 6.1 kHz
PSD (Vm^2/kHz)
favorable ITDs
unfavorable ITDs
Frequency [kHz]
C
LHS, plug in ipsi ear, 5.8 kHz
PSD (Vm^2/kHz)
favorable ITDs
unfavorable ITDs
Frequency [kHz]
B
% Maximum Amplitude
SNR, max 22.4
ITD [us]
D
% Maximum Amplitude
SNR, max 21.1
ITD [us]
E
SNR max
Control
L brain (plug)
R brain
Low
High
Frequency (kHz)
F
SNR max
Control
L brain
R brain
Low
High
Population
G
Estimated marginal means
Population: Low
Population: High
Control
R brain
L brain
H
Difference in BF (Oct)
L Stim
R Stim
Low
High
H*
Peak Cross Correlation (Oct)
Control
L brain
R brain
mean
median
Low
High

Figure 5

A

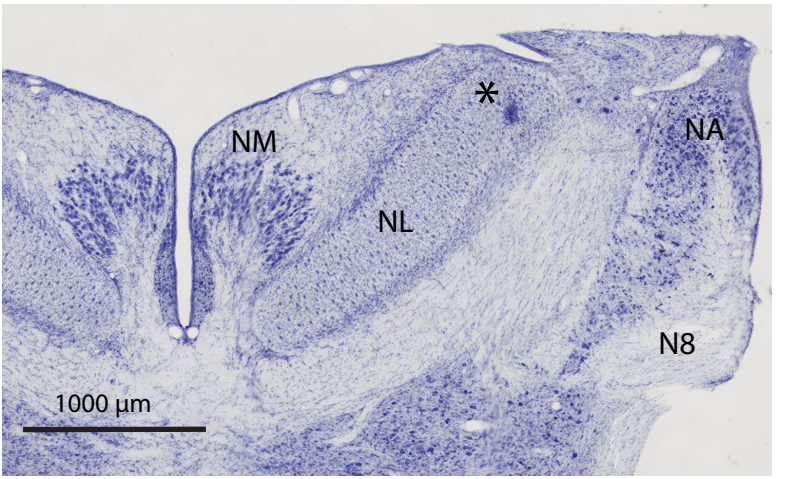
NM
NL
NA
N8
1000 µm

B

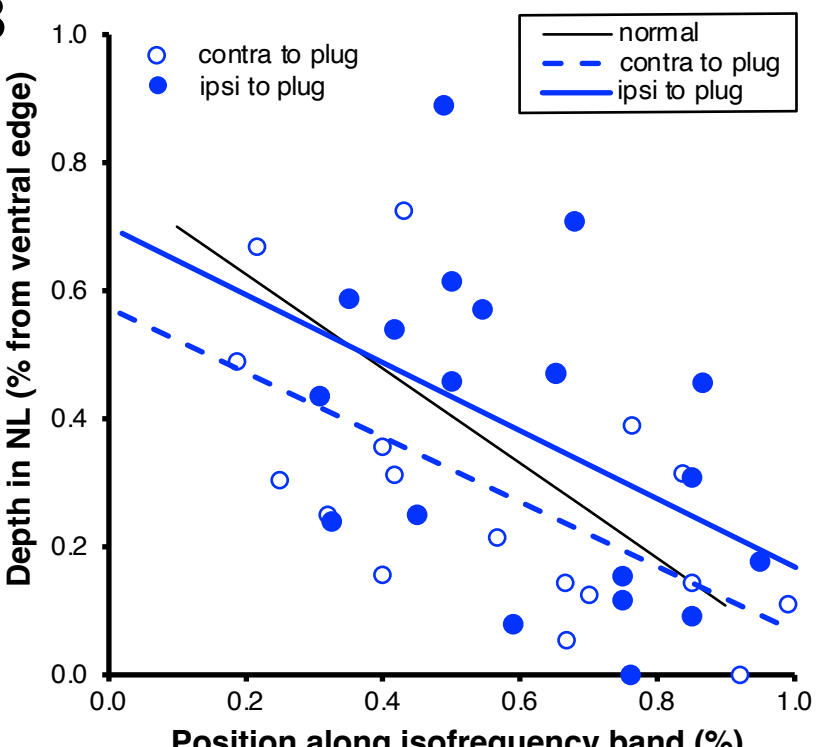
contra to plug
ipsi to plug
normal
contra to plug
ipsi to plug
Depth in NL (% from ventral edge)
Position along isofrequency band (%)
0.0
0.2
0.4
0.6
0.8
1.0